Asymptotically and exactly energy balanced Augmented flux-ADER schemes with application to hyperbolic conservation laws with geometric source terms

A. Navas-Montilla , J. Murillo [1]

anavas@unizar.es, Javier.Murillo@unizar.es, Fluid Mechanics. LIFTEC, CSIC-Universidad de Zaragoza. Zaragoza, Spain

Abstract

In this work, an arbitrary order HLL-type numerical scheme is constructed using the flux-ADER methodology. The proposed scheme is based on an augmented Derivative Riemann solver that was used for the first time in [A. Navas-Montilla, J. Murillo, Energy balanced numerical schemes with very high order. The Augmented Roe Flux ADER scheme. Application to the shallow water equations, J. Comput. Phys. 290 (2015) 188–218]. Such solver, hereafter referred to as Flux-Source (FS) solver, was conceived as a high order extension of the augmented Roe solver and led to the generation of a novel numerical scheme called AR-ADER scheme. Here, we provide a general definition of the FS solver independently of the Riemann solver used in it. Moreover, a simplified version of the solver, referred to as Linearized-Flux-Source (LFS) solver, is presented. This novel version of the FS solver allows to compute the solution without requiring reconstruction of derivatives of the fluxes, nevertheless some drawbacks are evidenced. In contrast to other previously defined Derivative Riemann solvers, the proposed FS and LFS solvers take into account the presence of the source term in the resolution of the Derivative Riemann Problem (DRP), which is of particular interest when dealing with geometric source terms. When applied to the shallow water equations, the proposed HLLS-ADER and AR-ADER schemes can be constructed to fulfill the exactly well-balanced property, showing that an arbitrary quadrature of the integral of the source inside the cell does not ensure energy balanced solutions. As a result of this work, energy balanced flux-ADER schemes that provide the exact solution for steady cases and that converge to the exact solution with arbitrary order for transient cases

are constructed.

Keywords: ADER, HLL solver, Energy balanced, Shallow water, Source terms, High order accuracy.

---

1. Introduction

Finite volume numerical schemes have experienced a great improvement in the resolution of complex flows over the past few decades. The keystone of such improvement is the preservation of high accuracy in both space and time when computing the solution. The ideas of ENO and WENO reconstructions [2, 3] supposed a major step when seeking high order in space, however, the preservation of high order in time was generally done by means of a Runge-Kutta time discretization, which proved to be inefficient for very high orders of accuracy [4]. This issue was addressed when using the ADER approach [5, 6], which can be regarded as a high order generalization of Godunov's method by means of a Taylor power series expansion of the numerical fluxes and source term. ADER schemes are fully discrete and consist of two main steps: first, a high-order spatial reconstruction procedure and secondly the resolution of a high order extension of the Riemann problem (RP). ADER schemes successfully allow the construction of arbitrary order schemes for systems of hyperbolic conservation laws [7, 8, 9].

In the framework of ADER schemes, a high order generalization of the Riemann Problem is required. It is well known that RPs are initial value problems (IVP) whose initial condition is given by piecewise functions and whose solution is used to estimate the numerical fluxes required for Godunov's scheme. This classic RP can be regarded as a first order approach to a Cauchy problem. A second order approach (with piecewise linear data) to the Cauchy problem was introduced by Ben-Artzi and Falcovitzin [10] and termed by them as Generalized Riemann Problem (GRP). More generally, an arbitrary order approach to the Cauchy problem is given by the Derivative Riemann Problem (DRP), where the initial condition consists of piecewise polynomial data with K nontrivial derivatives. Such polynomials are usually constructed by means of the aforementioned ENO or WENO reconstruction procedures. DRP with initial data composed of polynomials with K nontrivial derivatives will be referred to as DRP_K and allows to construct a K-th order ADER scheme.

An approach for the resolution of the DRP_K was first presented in [7] and

the proposed solver was called Toro–Titarev (TT) solver. In this work, the authors consider that the DRP may also contain source terms, which is another difference with respect to the GRP of Ben-Artzi and Falcovitzin. This solver is based on the construction of a time-dependent solution at the interface as a power series expansion in time. The leading term of the expansion is given by the solution of a conventional RP whose initial condition is given by a K-th order reconstruction of the conserved quantities at each side of the interface. The higher order terms of the expansion require the computation of time derivatives, for which the Cauchy-Kowalewski procedure is used. It is worth emphasizing that the TT approach allows to reduce the DRP_K to a series of classical Riemann problems where classic Riemann solvers are of application. The DRP_K consist of one RP for the leading term, referred to as DRP_0, plus K additional RPs for the derivatives. The RP for the leading term may be non-linear while the K RPs for the derivatives are linearized versions.

Apart from the TT solver, a wide variety of Derivative Riemann solvers have been designed to provide accurate numerical solutions for many non-linear problems under a diversity of conditions. For instance, we find in the literature the HEOC solver [11], constructed as a reinterpretation of the method of Harten et al. [2] and the the Castro–Toro (CT) solver [11], which results from a modification of both the HEOC and the TT solvers. To deal with stiff source terms, Toro and Montecinos proposed an implicit version of the TT and HEOC solvers in [12] and Dumbser et al. proposed a novel method, called DET solver [13], which uses a local space-time discontinuous Galerkin (DG) scheme for the time-evolution part of the algorithm, instead of using the Cauchy–Kovalewski procedure. At the same time, a novel solver called Flux-Source (FS) solver was presented in [1], together with the AR-ADER scheme, as a high order extension of the augmented Roe solver in [14]. The TT, CT, HEOC and FS solvers make use of Taylor series expansions and the Cauchy–Kowalewski procedure to provide a good estimation of the evolved states, whereas the DET solver is designed to evolve the data by using discontinuous Galerkin finite elements. The DET solver was proven to have an enhanced performance when dealing with stiff source terms [13].

When considering the three first solvers, similarities among them are worth being mentioned. For such solvers, it is assumed that the two initial states, separated by a discontinuity at the origin, lead to a single solution connecting the two initial states, referred to as the star solution [15]. They compute the intercell numerical fluxes using the time-integral average of the

time-dependent star solution. Nevertheless, they do consider different strategies to compute the evolution of the states and hence the star solution.

In the TT and CT solvers, the time-dependent star solution is computed adopting the so-called state expansion approach. Such technique proposes the construction of the solution as a Taylor power series expansion in time. The leading term of the expansion is given by the solution of a classical Riemann problem for the evolution of the conserved quantities neglecting the presence of the source term. The calculation of the higher order terms varies from one solver to the other. In the TT solver, the higher order terms are constructed using space derivatives by means of the Cauchy–Kowalewski procedure. Those spatial derivatives are evolved by solving conventional homogeneous linearized Riemann problems without source terms for spatial derivatives of the conserved quantities. On the other hand, in the CT solver the higher order terms are directly given by the solution of conventional homogeneous linearized Riemann problems without source terms for time derivatives. In this case, the Cauchy–Kowalewski procedure is used to provide the initial data for such RPs. A radically different approach is used in the HEOC solver, which only considers the resolution of conventional homogeneous non-linear RPs whose initial data has already been evolved separately in time by means of Taylor power series expansions. The Cauchy–Kowalewski procedure is used in this case to provide an estimation of left and right time derivatives at the initial time that are used to compose the aforementioned expansions.

Alternatively to the calculation of the star solution as a power series expansion in time for a further evaluation of the numerical flux, as done in the TT-ADER and CT-ADER schemes, it is possible to directly compute the numerical flux as as a Taylor power series expansion in time of the fluxes at the interface. Such schemes are referred to as flux-expansion ADER schemes. That is the case of the AR-ADER scheme presented in [1] for the first time.

There is a wide variety of physical problems modelled by non-homogeneous systems of balance laws commonly dominated by the source terms. For such problems, the treatment of the source terms in the numerical scheme is of utmost importance in order to provide realistic and physically feasible solutions. In this work, we focus on the shallow water equations (SWE), which is a useful model to provide realistic predictions in large variety of environmental flows. According to [11, 16, 17, 18], ADER schemes have proven to be suitable for the resolution of the SWE.

As outlined before, TT, CT and HEOC solvers consider a single solution

between the initial states and therefore difficulties may arise when seeking an exact balance of fluxes and sources when dealing with source terms of a certain nature. That is the case of the so-called geometric source terms, which appear for instance when modelling the thrust exerted by the variation of the bed level elevation in the SWE. For this kind of sources it is necessary to account for the jump of the geometric quantity across the cell edge and, to this end, augmented solvers were introduced.

Augmented solvers [19] were created to adequately characterize the influence of the source terms in the numerical solution and to explain the effect of the source terms in the stability region [20, 21]. The source term is accounted for in the numerical solution as an extra stationary wave at the interface. Due to the presence of the new wave, two solutions appear now at each side of the initial discontinuity instead of having a single star region. Based on the widespread Roe solver defined for homogeneous RPs in [22], an augmented version of the solver, named ARoe solver, was presented in [14]. Analogously, by adding an extra wave to the formulation of the original HLL and HLLC solvers [23, 24], two augmented solvers of the HLL type, named HLLS and HLLCS, were presented in [25].

In this work, we revisit and provide a complete description of the FS solver presented in [1], which is an arbitrary-order augmented Derivative Riemann solver. Such solver was presented for the first time in combination with the ARoe solver and the resulting numerical scheme was termed by the authors AR-ADER scheme. This scheme can be regarded as an arbitrary order extension of the ARoe method in [14]. The FS solver, like the CT and TT solvers, allows to decompose the DRP_K in one RP for the leading term plus K additional RPs composed of the evolution equation of time derivatives. However, unlike in the CT and TT solver, all RPs are considered now non-linear and non-homogeneous, as they include the source term. The construction of the FS solver can be regarded as the natural arbitrary-order generalization of a first-order augmented solver. The sought solution for each RP is the k-th numerical flux associated to each single RP and is used to compose the Taylor power series expansion in time that approximates the intercell numerical flux.

A novel simplification of the FS solver, named Linearized Flux-Source (LFS) solver, is also presented in this work. Such approach considers an alternative approximation to the RPs associated to the evolution equations for derivatives. As mentioned before, the FS solver assumes a decomposition of the DRP in $K+1$ non-linear RPs. In the LFS solver, those RPs correspond-

ing to the derivatives are linearized by means of a suitable approximation of the Jacobian matrix at the initial time, leading to conventional linearized non-homogeneous RPs. Such strategy is done, for instance, in the TT and CT solvers, where linearized (but homogeneous) equations are solved. When using this approach, only time derivatives of the conserved quantities are required as initial data to obtain the solution of the RPs, avoiding the computation of time derivatives of the fluxes. However, it is done at the expense of a stronger restriction on the time step due to the linearization of the equations. Numerical experiments regarding this issue are included in this text.

In this work, we also present a novel ADER scheme that uses the FS solver in combination with the HLLS method. The resulting scheme will be called HLLS-ADER scheme and can be used for systems of 2 waves. Contrary to the AR-ADER scheme, the HLLS-ADER scheme can be considered fully nonlinear since it considers the full set of waves present in the exact solution of the evolution equations and the numerical flux is directly computed from the integral form of the governing equations.

Considering again the application to the SWE, is must be borne in mind that source terms require an especial treatment in order to provide physically based responses when reproducing steady and transient events. The still water at rest is considered an important case where the numerical scheme must provide a good performance. Numerical schemes able to preserve still water at rest are called well-balanced methods, concept introduced by Bermudez and Vázquez-Cendón [26] and Greenberg and Leroux [27]. There is a large variety of well-balanced methods based on Riemann solver techniques that ensure the preservation of the still water steady state [28, 29, 30, 31, 32, 33, 34, 35, 36, 37, 38, 39, 40, 41]. In [42], Caleffi et al. carried out an exhaustive study on the treatment of bed steps, both in the framework of classical finite volume and path conservative approach, when constructing well-balanced Discontinuous–Galerkin schemes.

When considering steady states with moving water over irregular geometries, the preservation of the C-property (exact conservation property) [43] is also important in order to provide an exact equilibrium between fluxes and source terms. Numerical methods preserving the C-property are able to ensure a uniform discharge value under steady conditions and can be constructed using flux-type definitions for the source terms [44, 20].

The performance of numerical schemes preserving the C-property can still be enhanced. If neglecting friction in the SWE, mechanical energy is

conserved under steady conditions in absence of hydraulic jumps. Such idea of energy conservation can be integrated in the numerical scheme in the discrete level, allowing the extension of well-balanced methods to exactly well-balanced methods [45, 46, 47, 48]. In [49, 50], exactly well-balanced methods using the ARoe and HLLS solvers were presented, reproducing the exact solution for steady states with independence of the cell size. Numerical methods in [49, 50] were called energy balanced numerical schemes. The keystone for the conservation of energy in the discrete level is found in the way source terms are discretized at cell interfaces, as they must be given the exact value to balance the difference of fluxes across the interfaces.

The AR-ADER scheme in [1] was constructed putting special emphasis in the preservation of the C-Property and also the energy balance property, so that the scheme provides the exact solution for steady cases with moving water and irregular geometries with independence of the grid geometry. Moreover, the mentioned scheme was able to ensure convergence to the exact solution for unsteady problems including RPs that involved bed variations and resonant solutions, including the limiting situation when the Riemann data belongs to the resonance hypersurface [35]. It is worth mentioning that in order to ensure such capabilities when constructing the numerical schemes, specific data reconstruction techniques were required. Initial data for the DRP_0 was reconstructed using WENO reconstruction procedures. The sub-cell derivative WENO reconstruction was chosen for space derivatives reconstruction and a suitable expression of the resulting functions when applying the Cauchy-Kowalevski procedure was evidenced to be required [1]. In this work, the same techniques are used.

On the other hand, we must point out that a suboptimal behavior of the AR-ADER scheme has been observed in certain cases for the water surface elevation. According to [45], the use of a low order approximation of the integral of the source term inside the cell is the reason of that behavior. The election of a suitable approximation of the integral of the source term is not a trivial task since it is necessary to use energy balanced discretizations to guarantee the conservation of energy in the discrete level and therefore traditional quadrature rules cannot be used. In this work, a high order generalization of the energy-balanced integration method in [49] is proposed, following [45]. This novel approach uses Richardson extrapolation technique to construct an arbitrary order approximation by means of composite energy-balanced integration over multiple sub-cell grids. Other ways of integration of the source term are explored in this work, allowing to construct asymptotically energy

balanced schemes that ensure convergence to the exact solution for steady and transient cases.

The outline of the paper is next presented. In section 2, an introduction to nonlinear systems of conservation laws with source terms is provided and the definition of geometric source terms is recalled. In Section 3, we present the basic structure of the flux-ADER schemes constructed in this work, recalling the definition of the DRP. At the end of the section, we provide a complete description of the FS solver for the first time and present the LFS solver. Chapter 4 is devoted to the AR-ADER solver presented in [1] including some improvements in the scheme. In addition, a novel version based on the LFS and called Augmented Roe Linear ADER (ARL-ADER) scheme, is presented. In Chapter 5, the HLLS-ADER scheme is presented for the first time, in both the flux and the fluctuation form. As done for the AR-ADER scheme, the linearized version of this scheme, called HLLS Linear ADER (HLLSL-ADER) method, is included. Chapter 6 is devoted to the application of the proposed schemes to the SWE and includes the numerical techniques to construct an energy balanced scheme. Numerical results are included in this chapter. Finally, in Chapter 7 we present a summary of the work and the concluding remarks.

2. Nonlinear systems of equations with source term

The basic ideas underlying this work can be illustrated by examining hyperbolic nonlinear systems of equations with source terms in 1D, that can be expressed in integral form as

$$\frac{\partial}{\partial t}\int_{x_1}^{x_2}\mathbf{U}dx + \mathbf{F}|_{x_2} - \mathbf{F}|_{x1} - \int_{x_1}^{x_2}\mathbf{S}dx = 0\,, \tag{1}$$

where x_1, x_2 are the limits of a generic control volume and with N_λ equations. Such systems arise naturally from the conservation laws for certain physical quantities in nature. The differential formulation is obtained when assuming a smooth variation of the variables and an infinitesimal width of the control volume, yielding

$$\frac{\partial \mathbf{U}}{\partial t} + \frac{\partial \mathbf{F}}{\partial x} = \mathbf{S}\,, \tag{2}$$

where $\mathbf{U} = \mathbf{U}(x,t) \in \mathcal{C} \subset \mathbb{R}^{N_\lambda}$ is the vector of conserved quantities that takes values on $\mathcal{C}$, the set of admissible states of $\mathbf{U}$, $\mathbf{F} = \mathbf{F}(\mathbf{U})$ is the flux

function that represents a nonlinear mapping of the conserved quantities from $\mathcal{C}$ to $\mathbb{R}^{N_\lambda}$ and $\mathbf{S}$ is the source term, that will be considered a function of the conserved quantities and spatial coordinate as $\mathbf{S} = \mathbf{S}(\mathbf{U}, x)$. In this work, we put a special emphasis on the so-called *geometric source terms*, that are expressed as

$$\mathbf{S}(\mathbf{U}, x) = \mathbf{S}_s(\mathbf{U}) \frac{d}{dx} \mathbf{S}_g(x) \,, \tag{3}$$

with $\mathbf{S}_s(\mathbf{U})$ a function of the conserved quantities and $\mathbf{S}_g(x)$ the geometric function that depends upon the position x and can be discontinuous.

From (2), it is possible to define a Jacobian matrix for the convective part as

$$\mathbf{J} = \frac{d\mathbf{F}(\mathbf{U})}{d\mathbf{U}} \,. \tag{4}$$

Assuming that the convective part in (2) is strictly hyperbolic, with N_λ real eigenvalues $\lambda^1, ..., \lambda^{N_\lambda}$ and eigenvectors $\mathbf{e}^1, ..., \mathbf{e}^{N_\lambda}$, it is possible define two matrices $\mathbf{P} = (\mathbf{e}^1, ..., \mathbf{e}^{N_\lambda})$ and $\mathbf{P}^{-1}$ with the property that they diagonalize the Jacobian $\mathbf{J}$

$$\mathbf{J} = \mathbf{P} \mathbf{\Lambda} \mathbf{P}^{-1} \,. \tag{5}$$

When the Jacobian matrix in (4) does not depend upon $\mathbf{U}$, the system in (2) is said to be *linear* and the flux function can be expressed as $\mathbf{F}(\mathbf{U}) = \mathbf{J}\mathbf{U}$ with $\mathbf{J}$ a constant matrix.

3. The Derivative Riemann Problem and Flux-ADER schemes

In this section, the theoretical framework for the construction of arbitrary order Goudunov-type numerical schemes is revisited. The methodology followed here is to construct arbitrary order schemes using the flux-ADER approach, which is based on a high order extension of Godunov's method by means of a Taylor power series expansion in time of the numerical fluxes and the source term. When dealing with ADER schemes, a generalization of the Riemann Problem is required to compute the numerical fluxes at cell interfaces. Such problem is the aforementioned DRP, recalled in Section 3.1. When solving the DRP, reconstruction of the conserved variables in time and space is required. In this work, WENO reconstruction procedures will

be used to carry out the spatial reconstruction while the temporal evolution of the variables will be computed by means of the Cauchy-Kowalevski procedure.

The finite volume discretization used in this work is next defined. Let us consider again the initial problem we want to solve, composed by the system in (2) in combination with a boundary condition and an initial condition. This problem is an initial boundary value problem, given by

$$\begin{cases} \dfrac{\partial \mathbf{U}}{\partial t} + \dfrac{\partial \mathbf{F}(\mathbf{U})}{\partial x} = \mathbf{S} \\ \\ \mathbf{U}(x,0) = \mathbf{U}_0(x) \\ \\ \mathbf{U}(a,t) = \mathbf{U}_a(t)\,, \quad \mathbf{U}(b,t) = \mathbf{U}_b(t) \end{cases} \tag{6}$$

defined inside the domain $[a,b] \times [0,T]$, with $\mathbf{U}_0(x)$ the initial condition and $\mathbf{U}_a(t)$ and $\mathbf{U}_b(t)$ the left and right boundary conditions. The computational grid is composed by N cells

$$a = x_{\frac{1}{2}} < x_{\frac{3}{2}} < ... < x_{N-\frac{1}{2}} < x_{N+\frac{1}{2}} = b\,, \tag{7}$$

as shown in Figure 1, with cells and cell sizes defined as

$$\Omega_i = \left[x_{i-\frac{1}{2}}, x_{i+\frac{1}{2}} \right], \qquad i = 1, ..., N\,, \tag{8}$$

$$\Delta x_i = x_{i+\frac{1}{2}} - x_{i-\frac{1}{2}}\,, \qquad i = 1, ..., N\,, \tag{9}$$

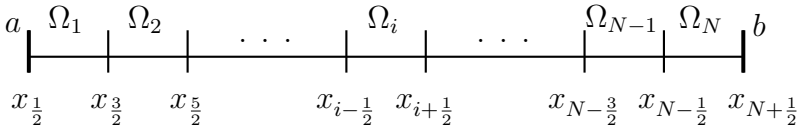

Figure 1: Mesh discretization

Inside each cell, the conserved quantities are defined as cell averages as

$$\mathbf{U}_i^n = \frac{1}{\Delta x_i} \int_{x_{i-\frac{1}{2}}}^{x_{i+\frac{1}{2}}} \mathbf{U}(x, t^n) dx \qquad i = 1, ..., N\,. \tag{10}$$

3.1. The Derivative Riemann Problem

An arbitrary order approach to the Cauchy problem is given by the DRP_K, that is an IVP defined by a system of N_λ EDPs and an initial condition consisting of piecewise polynomial data with K nontrivial derivatives, separated by a single discontinuity at $x = 0$

$$\begin{cases} \dfrac{\partial \mathbf{U}}{\partial t} + \dfrac{\partial \mathbf{F}(\mathbf{U})}{\partial x} = \mathbf{S} \\ \\ \mathbf{U}(x,0) = \begin{cases} \mathbf{U}_i(x) & x < 0 \\ \mathbf{U}_{i+1}(x) & x > 0 \end{cases} \end{cases} \tag{11}$$

The initial states, $\mathbf{U}_i(x)$ and $\mathbf{U}_{i+1}(x)$, are smooth functions of distance x and can be defined using suitable reconstruction procedures at the initial time. Recall that x stands for the local spatial coordinate, centered at $x_{i+1/2}$. Theoretical aspects regarding the DRP can be found in [51]. DRP in (11) is depicted in Figure 2 for the case when $N_\lambda = 2$.

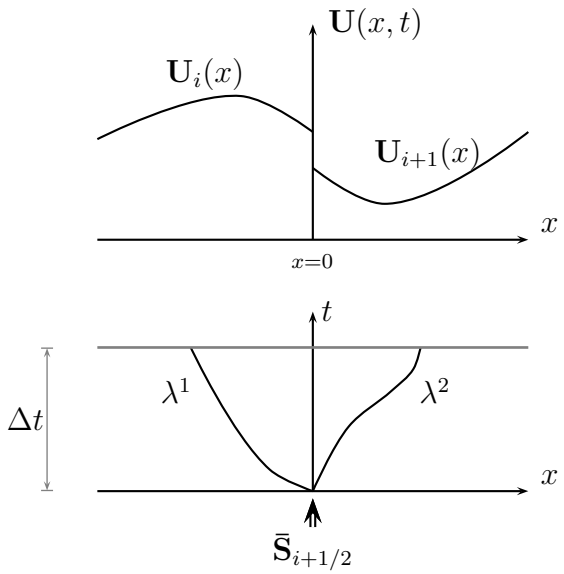

Figure 2: Graphical representation of the DRP_K showing the piecewise smooth states (upper figure) and wave velocities that depend upon time (lower figure).

For DRP in (11), it is possible to define the following values for vector $\mathbf{U}$ at the interface

$$\mathbf{U}_{i_R}^{(0)} = \lim_{x\to 0^-} \mathbf{U}_i(x)\,, \qquad \mathbf{U}_{(i+1)_L}^{(0)} = \lim_{x\to 0^+} \mathbf{U}_{i+1}(x) \tag{12}$$

and for its derivatives

$$\mathbf{U}_{i_R}^{(k)} = \lim_{x\to 0^-} \frac{\partial^k}{\partial x^k}\mathbf{U}_i(x)\,, \qquad \mathbf{U}_{(i+1)_L}^{(k)} = \lim_{x\to 0^+} \frac{\partial^k}{\partial x^k}\mathbf{U}_{i+1}(x)\,, \tag{13}$$

at the initial time, with $k = 1, ..., K$.

Analogously, it is possible to define the following values for the physical fluxes $\mathbf{F}(\mathbf{U})$ at the interface

$$\mathbf{F}_{i_R}^{(0)} = \lim_{x\to 0^-} \mathbf{F}(\mathbf{U}_i(x))\,, \qquad \mathbf{F}_{(i+1)_L}^{(0)} = \lim_{x\to 0^+} \mathbf{F}(\mathbf{U}_{i+1}(x)) \tag{14}$$

and for their spatial derivatives

$$\mathbf{F}_{i_R}^{(k)} = \lim_{x\to 0^-} \frac{\partial^k}{\partial x^k}\mathbf{F}(\mathbf{U}_i(x))\,, \qquad \mathbf{F}_{(i+1)_L}^{(k)} = \lim_{x\to 0^+} \frac{\partial^k}{\partial x^k}\mathbf{F}(\mathbf{U}_{i+1}(x))\,, \tag{15}$$

at the initial time, with $k = 1, ..., K$.
The spatial reconstruction of the source term $\mathbf{S}(\mathbf{U}, x, t)$ will be denoted in the same way

$$\mathbf{S}_{i_R}^{(0)} = \lim_{x\to 0^-} \mathbf{S}(\mathbf{U}_i(x), x, 0)\,, \qquad \mathbf{S}_{(i+1)_L}^{(0)} = \lim_{x\to 0^+} \mathbf{S}(\mathbf{U}_{i+1}(x), x, 0) \tag{16}$$

and also its derivatives

$$\mathbf{S}_{i_R}^{(k)} = \lim_{x\to 0^-} \frac{\partial^k}{\partial x^k}\mathbf{S}(\mathbf{U}_i(x), x, 0)\,, \qquad \mathbf{S}_{(i+1)_L}^{(k)} = \lim_{x\to 0^+} \frac{\partial^k}{\partial x^k}\mathbf{S}(\mathbf{U}_{i+1}(x), x, 0)\,, \tag{17}$$

at the initial time, with $k = 1, ..., K$.

The value of $\mathbf{U}$ at the center of each cell will be denoted as $\mathbf{U}_i^0 = \mathbf{U}_i(x_i)$. Subscripts L and R are defined with reference to the cell center, as depicted in Figure 3.

High order numerical methods of the flux-ADER type require the numerical fluxes at the interface position $x_{i+1/2}$ as a function of time t, allowing to compute their integral average and construct a numerical scheme of $K+1$-th order of accuracy in both space and time. Following [52] the solution

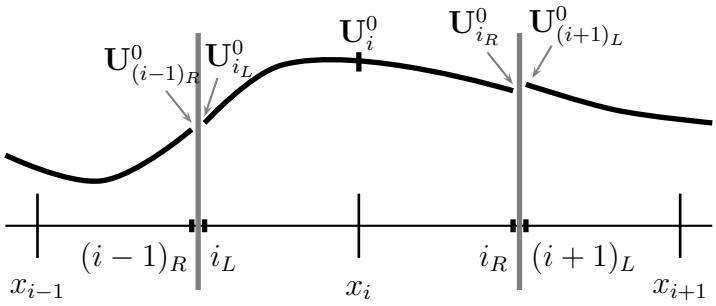

Figure 3: Mesh discretization

will contain a leading term, provided by the DRP_0, equivalent to the classical piecewise constant data Riemann problem, associated with the first order Godunov scheme [53] and higher-order terms, associated with the K different RPs for the derivatives.

3.1.1. Evolution equation for derivatives

DRP in (11) provides the evolution equation for variable $\mathbf{U}$. Evolution equations for spatial or time derivatives of $\mathbf{U}$, denoted by $\partial_x^{(k)}\mathbf{U}$ and $\partial_t^{(k)}\mathbf{U}$ respectively, will be required for the resolution of the DRP. In this work, we will only solve the evolution of time derivatives. Such equations are straightforward obtained by taking succesive derivatives of (2), yielding

$$\frac{\partial}{\partial t}\left(\partial_t^{(k)}\mathbf{U}\right) + \frac{\partial}{\partial x}\left(\partial_t^{(k)}\mathbf{F}(\mathbf{U})\right) = \partial_t^{(k)}\mathbf{S} \qquad k = 1, ..., K\,. \tag{18}$$

3.1.2. Cauchy-Kowalevski Theorem

When dealing with EDPs of the type of (2), relations between temporal and spatial derivatives of $\mathbf{U}$ are provided by the Cauchy-Kowalevski Theorem. Here, it is used to derive analytic expressions for time derivatives of $\mathbf{F}$ and $\mathbf{U}$ departing from the information provided by the spatial reconstruction method. It allows to express time derivatives of the physical fluxes at $t = 0$ as functions $\mathbf{R}^{(k)}$ of spatial derivatives of $\mathbf{U}$ and $\mathbf{S}$

$$\partial_t^{(k)}\mathbf{F} = \mathbf{R}^{(k)}(\partial_x^{(k)}\mathbf{U}, \partial_x^{(k-1)}\mathbf{U}, ..., \mathbf{U}, \partial_x^{(k)}\mathbf{S}, \partial_x^{(k-1)}\mathbf{S}, ..., \mathbf{S})\,. \tag{19}$$

Spatial derivatives defined at the cell interface $i+1/2$ in (13) are calculated using the sub-cell WENO derivative reconstruction method [54]. They allow to compute the values of $\mathbf{R}^{(k)}$ at each side of the discontinuity in the DRP_K

$$\mathbf{R}^{(k)}_{i_R} = \lim_{x\to 0^-} \mathbf{R}^{(k)} \approx \mathbf{R}^{(k)}(\mathbf{U}^{(k)}, \mathbf{U}^{(k-1)}, ..., \mathbf{U}^0, \mathbf{S}^{(k)}, \mathbf{S}^{(k-1)}, ..., \mathbf{S}^0)_{i_R}\,,$$

$$\mathbf{R}^{(k)}_{(i+1)_L} = \lim_{x\to 0^+} \mathbf{R}^{(k)} \approx \mathbf{R}^{(k)}(\mathbf{U}^{(k)}, \mathbf{U}^{(k-1)}, ..., \mathbf{U}^0, \mathbf{S}^{(k)}, \mathbf{S}^{(k-1)}, ..., \mathbf{S}^0)_{(i+1)_L}\,. \tag{20}$$

Analogously, it is possible to construct temporal derivatives of $\mathbf{U}$ at $t=0$ as functions $\mathbf{D}^{(k)}$ of spatial derivatives of $\mathbf{U}$ and $\mathbf{S}$

$$\partial_t^{(k)}\mathbf{U} = \mathbf{D}^{(k)}(\partial_x^{(k)}\mathbf{U}, \partial_x^{(k-1)}\mathbf{U}, ..., \mathbf{U}, \partial_x^{(k)}\mathbf{S}, \partial_x^{(k-1)}\mathbf{S}, ..., \mathbf{S})\,, \tag{21}$$

allowing to compute the values of $\mathbf{D}^{(k)}$ at each side of the discontinuity in the DRP_K

$$\mathbf{D}^{(k)}_{i_R} = \lim_{x\to 0^-} \mathbf{D}^{(k)} \approx \mathbf{D}^{(k)}(\mathbf{U}^{(k)}, \mathbf{U}^{(k-1)}, ..., \mathbf{U}^0, \mathbf{S}^{(k)}, \mathbf{S}^{(k-1)}, ..., \mathbf{S}^0)_{i_R}\,,$$

$$\mathbf{D}^{(k)}_{(i+1)_L} = \lim_{x\to 0^+} \mathbf{D}^{(k)} \approx \mathbf{D}^{(k)}(\mathbf{U}^{(k)}, \mathbf{U}^{(k-1)}, ..., \mathbf{U}^0, \mathbf{S}^{(k)}, \mathbf{S}^{(k-1)}, ..., \mathbf{S}^0)_{(i+1)_L}\,. \tag{22}$$

Temporal derivatives of the source term, $\mathbf{S}$, at $t=0$ can also be obtained using the Cauchy-Kowalevski procedure as functions $\mathbf{Q}^{(k)}$ of spatial derivatives of $\mathbf{U}$ and $\mathbf{S}$

$$\partial_t^{(k)}\mathbf{S} = \mathbf{Q}^{(k)}(\partial_x^{(k)}\mathbf{U}, \partial_x^{(k-1)}\mathbf{U}, ..., \mathbf{U}, \partial_x^{(k)}\mathbf{S}, \partial_x^{(k-1)}\mathbf{S}, ..., \mathbf{S})\,. \tag{23}$$

3.2. Finite volume discretization and Flux-ADER schemes

Following the approach proposed by Godunov, a suitable arbitrary-order discretization of the system in (2) inside $[x_{i-1/2}, x_{i+1/2}]\times[t^n, t^{n+1}]$ can be expressed as

$$\mathbf{U}_i^{n+1} = \mathbf{U}_i^n - \frac{\Delta t}{\Delta x}[\mathbf{F}^-_{i+1/2} - \mathbf{F}^+_{i-1/2}] + \frac{\Delta t}{\Delta x}[\bar{\mathbf{S}}_{i_R,i_L}]\,, \tag{24}$$

with the numerical fluxes $\mathbf{F}^-_{i+1/2}$ and $\mathbf{F}^+_{i-1/2}$ defined as time-integral averages of the time-dependent fluxes evolved in time at the interfaces

$$\mathbf{F}^{-}_{i+1/2} = \frac{1}{\Delta t}\int_0^{\Delta t} \mathbf{F}^{-}_{i_R}(\tau)\, d\tau\,, \qquad \mathbf{F}^{+}_{i-1/2} = \frac{1}{\Delta t}\int_0^{\Delta t} \mathbf{F}^{+}_{i_L}(\tau)\, d\tau \tag{25}$$

and $\bar{\mathbf{S}}_{i_R,i_L}$ a suitable approximation of the integral of the source term inside the cell given by

$$\bar{\mathbf{S}}_{i_R,i_L} \approx \frac{1}{\Delta t}\int_0^{\Delta t}\int_{x_{i_L}}^{x_{i_R}} \mathbf{S}\; dx\; d\tau\,. \tag{26}$$

Analogously, equation (24) can be rewritten in terms of fluctuations, generally denoted by $\delta\mathbf{M}$, leading to

$$\mathbf{U}_i^{n+1} = \mathbf{U}_i^{n} - \frac{\Delta t}{\Delta x}[\delta\mathbf{M}^{-}_{i+1/2} + \delta\mathbf{M}_{i_R,i_L} + \delta\mathbf{M}^{+}_{i-1/2}]\,, \tag{27}$$

where

$$\begin{aligned}
\delta\mathbf{M}^{-}_{i+1/2} &= \mathbf{F}^{-}_{i+1/2} - \frac{1}{\Delta t}\int_0^{\Delta t} \mathbf{F}_{i_R}(\tau)\, d\tau\,,\\
\delta\mathbf{M}_{i_R,i_L} &= \frac{1}{\Delta t}\int_0^{\Delta t} \mathbf{F}_{i_R}(\tau)\, d\tau - \frac{1}{\Delta t}\int_0^{\Delta t} \mathbf{F}_{i_L}(\tau)\, d\tau - \bar{\mathbf{S}}_{i_R,i_L}\,,\\
\delta\mathbf{M}^{+}_{i-1/2} &= \frac{1}{\Delta t}\int_0^{\Delta t} \mathbf{F}_{i_L}(\tau)\, d\tau - \mathbf{F}^{+}_{i-1/2}\,,
\end{aligned} \tag{28}$$

represent the contribution of the incoming waves to the right edge, the contribution due to the variation of the physical flux and source along the cell and the contribution of the incoming waves to the left edge, respectively. It is worth mentioning that fluctuation $\delta\mathbf{M}_{i_R,i_L}$ can be divided in as many terms as desired by making use of the telescopic property. For an arbitrary number of contributions, n_m, the centered fluctuation reads

$$\delta\mathbf{M}_{i_R,i_L} = \delta\mathbf{M}_{i_1,i_L} + \sum_{j=2}^{n_m-1} \delta\mathbf{M}_{i_j,i_{j-1}} + \delta\mathbf{M}_{i_R,i_{n_m-1}}\,, \tag{29}$$

requiring thus, extra inner cell information that may be provided by reconstruction procedures.

When the scheme in (27) is reduced to first order of accuracy, it is worth saying that the centered fluctuation, $\delta\mathbf{M}_{i_R,i_L}$, will be reduced to $\delta\mathbf{M}_{i_R,i_L} = \bar{\mathbf{S}}_{i_R,i_L}$ since the flux is constant inside the cell. In the case of using augmented Riemann solvers and a first order of accuracy, we must set $\delta\mathbf{M}_{i_R,i_L} = 0$ since the source term will be already accounted for in the weak solution of the RPs at the interfaces provided by the solver.

Physical fluxes at left and right cell edges, $\mathbf{F}_{i_L}(\tau)$ and $\mathbf{F}_{i_R}(\tau)$, can be approximated by a Taylor power series expansion in time as

$$\mathbf{F}_{i_L}(\tau) = \mathbf{F}_{i_L}^{(0)} + \sum_{k=1}^{K} \mathbf{R}_{i_L}^{(k)} \frac{\tau^k}{k!}\,, \qquad \mathbf{F}_{i_R}(\tau) = \mathbf{F}_{i_R}^{(0)} + \sum_{k=1}^{K} \mathbf{R}_{i_R}^{(k)} \frac{\tau^k}{k!}\,, \tag{30}$$

with $\mathbf{F}_{i_L}^{(0)}$ and $\mathbf{F}_{i_R}^{(0)}$ the so-called leading terms, computed as in (14) and with $\mathbf{R}_{i_L}^{(k)}$ and $\mathbf{R}_{i_R}^{(k)}$ the coefficients of the high order terms, computed as in (20).

As done for the fluxes, the source term inside cell Ω_i can also be approximated by a truncated Taylor power series expansion in time

$$\mathbf{S}_i(x,\tau) = \mathbf{S}_i(x,0) + \sum_{k=1}^{K} \left[\frac{\partial^k \mathbf{S}_i}{\partial t^k}\right]_{x,t=0} \frac{\tau^k}{k!}\,, \tag{31}$$

leading to the following expression for its integral inside the cell

$$\bar{\mathbf{S}}_{i_R,i_L} = \bar{\mathbf{S}}_{i_R,i_L}^{(0)} + \sum_{k=1}^{K} \bar{\mathbf{S}}_{i_R,i_L}^{(k)}\,, \tag{32}$$

with

$$\begin{aligned} \bar{\mathbf{S}}_{i_R,i_L}^{(0)} &= \frac{1}{\Delta t} \int_0^{\Delta t} \int_{x_{i_L}}^{x_{i_R}} \mathbf{S}_i(x,0)\; dx\; dt\,, \\ \bar{\mathbf{S}}_{i_R,i_L}^{(k)} &= \frac{1}{\Delta t} \int_0^{\Delta t} \int_{x_{i_L}}^{x_{i_R}} \left[\frac{\partial^k \mathbf{S}_i}{\partial t^k}\right]_{x,t=0} \frac{t^k}{k!}\; dx\; dt\,, \end{aligned} \tag{33}$$

that will be integrated by means of approximated quadrature rules.

As outlined before, when dealing with geometric source terms of the type of (3), the contribution of the source is not only accounted for inside the cell but also at cell interfaces [14, 1] so that the scheme converges to the exact

solution. In this case, the integral of the source and its derivatives has to be calculated at cell interfaces as

$$\begin{aligned}\bar{\mathbf{S}}^{(0)}_{i+1/2} &= \frac{1}{\Delta t}\int_0^{\Delta t}\int_{x^-_{i+1/2}}^{x^+_{i+1/2}} \mathbf{S}(x,0)\; dx\; dt\,,\\ \bar{\mathbf{S}}^{(k)}_{i+1/2} &= \frac{1}{\Delta t}\int_0^{\Delta t}\int_{x^-_{i+1/2}}^{x^+_{i+1/2}} \left[\frac{\partial^k \mathbf{S}_i}{\partial t^k}\right]_{x,t=0} dx\; dt\,,\end{aligned} \tag{34}$$

that will be integrated using suitable approximations.

3.3. The FS and LFS solvers

In this work, we recall and provide a general definition of the FS Derivative Riemann solver [1]. When using this solver, the DRP_K in (11) can be decomposed in $K+1$ conventional RPs, one for the evolution of the conserved quantities and K more problems for the evolution of the derivatives. The former is known as DRP_0 and corresponds to the following non-linear and non-homogeneous RP

$$\begin{cases} \dfrac{\partial \mathbf{U}}{\partial t} + \dfrac{\partial \mathbf{F}(\mathbf{U})}{\partial x} = \mathbf{S} \\ \mathbf{U}(x,0) = \begin{cases} \mathbf{U}^{(0)}_{i_R} & \text{if} \quad x<0 \\ \mathbf{U}^{(0)}_{(i+1)_L} & \text{if} \quad x>0 \end{cases} \end{cases} \tag{35}$$

with the sought solution for the fluxes denoted as $\mathbf{F}^{-,(0)}_{i_R}$ and $\mathbf{F}^{+,(0)}_{(i+1)_L}$.

The K RPs associated to the high order terms of the DRP_K are composed of the evolution equations for time derivatives of the conserved variables. The evolution equations for the derivatives are derived straightforward by differentiating the original system according to equation (18), leading to the following RP

$$\begin{cases} \dfrac{\partial}{\partial t}\left(\partial_t^{(k)}\mathbf{U}\right) + \dfrac{\partial}{\partial x}\left(\partial_t^{(k)}\mathbf{F}(\mathbf{U})\right) = \partial_t^{(k)}\mathbf{S} \\ \partial_t^{(k)}\mathbf{U}(x,0) = \begin{cases} \mathbf{D}^{(k)}_{i_R} & \text{if} \quad x<0 \\ \mathbf{D}^{(k)}_{(i+1)_L} & \text{if} \quad x>0 \end{cases} \end{cases} \tag{36}$$

with the sought solution for the fluxes denoted as $\mathbf{F}^{-,(k)}_{i_R}$ and $\mathbf{F}^{+,(k)}_{(i+1)_L}$. It is worth saying that the reconstructed time derivatives of the fluxes at the interfaces, $\mathbf{R}^{(k)}_{i_R}$ and $\mathbf{R}^{(k)}_{(i+1)_L}$, are also required when solving (36).

In this work, an alternative strategy in the resolution of the DRP is studied, leading to a new version of the FS solver. A similar strategy has been used by other authors [7, 11] and considers the resolution of linearized evolution equations for the derivatives. In [7, 11] linearized and homogeneous RPs for the derivatives are solved, however, the proposed simplification of the FS solver will consider linear but non-homogeneous RPs. The resulting method of resolution will be referred to as Linearized Flux-Source (LFS) Derivative Riemann solver. This approach only requires the reconstruction of time derivatives of the conserved quantities at the interfaces, unlike the FS solver that also requires time derivatives of the fluxes. In this case, we solve the following linearized RP for the evolution equations

$$\begin{cases} \dfrac{\partial}{\partial t}\left(\partial_t^{(k)}\mathbf{U}\right) + \widetilde{\mathbf{J}}_{i+1/2}\dfrac{\partial}{\partial x}\left(\partial_t^{(k)}\mathbf{U}\right) = \partial_t^{(k)}\mathbf{S} \\ \\ \partial_t^{(k)}\mathbf{U}(x,0) = \begin{cases} \mathbf{D}^{(k)}_{i_R} & \text{if} \quad x<0 \\ \mathbf{D}^{(k)}_{(i+1)_L} & \text{if} \quad x>0 \end{cases} \end{cases} \tag{37}$$

where $\widetilde{\mathbf{J}}_{i+1/2} = \tilde{\mathbf{J}}_{i+1/2}(\mathbf{U}^{(0)}_{i_R}, \mathbf{U}^{(0)}_{(i+1)_L})$ is a constant matrix that allows to approximate time derivatives of the flux as

$$\partial_t^{(k)}\mathbf{F}(\mathbf{U}) = \widetilde{\mathbf{J}}_{i+1/2}\partial_t^{(k)}\mathbf{U}\,. \tag{38}$$

Notice that the source term is not neglected as in the TT, CT and HEOC solvers [7, 11, 2]. As the constructed ADER schemes are of the flux-ADER type, only the solution for the fluxes will be sought when solving the DRP_K in (11).

When adopting the flux-expansion ADER approach we seek a truncated Taylor time expansion of the updated fluxes at the interfaces as

$$\mathbf{F}^{-}_{i_R}(\tau) = \mathbf{F}^{-,(0)}_{i_R} + \sum_{k=1}^{K}\mathbf{F}^{-,(k)}_{i_R}\frac{\tau^k}{k!}\,, \qquad \mathbf{F}^{+}_{(i+1)_L}(\tau) = \mathbf{F}^{+,(0)}_{(i+1)_L} + \sum_{k=1}^{K}\mathbf{F}^{+,(k)}_{(i+1)_L}\frac{\tau^k}{k!}\,, \tag{39}$$

that after integration, leads to the following expression of the numerical fluxes

$$\mathbf{F}^{-}_{i+1/2} = \mathbf{F}^{-,0}_{i_R} + \sum_{k=1}^{K} \mathbf{F}^{-,(k)}_{i_R} \frac{\Delta t^k}{(k+1)!}\,, \qquad \mathbf{F}^{+}_{i+1/2} = \mathbf{F}^{+,0}_{(i+1)_L} + \sum_{k=1}^{K} \mathbf{F}^{+,(k)}_{(i+1)_L} \frac{\Delta t^k}{(k+1)!}\,, \tag{40}$$

where $\mathbf{F}^{-,(0)}_{i_R}$ and $\mathbf{F}^{+,(0)}_{(i+1)_L}$ are computed from (35) and $\mathbf{F}^{-,(k)}_{i_R}$ and $\mathbf{F}^{+,(k)}_{(i+1)_L}$ are computed from (36) or (37).

4. The AR-ADER scheme

A flux-ADER type numerical scheme for the resolution of nonlinear systems of conservation laws with source terms called Augmented Roe ADER (AR-ADER) scheme was presented in [1]. This scheme was constructed following the flux-ADER approach, that is, instead of searching solutions of the conserved quantities at both sides of the interface to evaluate the fluxes, approximate intercell numerical fluxes were sought. Special emphasis was put on the discretization and incorporation of the source term in the solution of the DRP_K, when dealing with geometric source terms of the type of (3). In this section, the scheme presented in [1] is revisited.

Let us consider the hyperbolic nonlinear system of equations with source term in (2). Assuming that the convective part of (2) is strictly hyperbolic, with N_λ real eigenvalues $\lambda^1, ..., \lambda^{N_\lambda}$ and eigenvectors $\mathbf{e}^1, ..., \mathbf{e}^{N_\lambda}$, it is possible define two matrices $\mathbf{P} = (\mathbf{e}^1, ..., \mathbf{e}^{N_\lambda})$ and $\mathbf{P}^{-1}$ with the property that they diagonalize the Jacobian $\mathbf{J}$, as shown in (5).

As outlined in the previous section, the expression for the updating scheme is constructed as

$$\mathbf{U}^{n+1}_i = \mathbf{U}^n_i - \frac{\Delta t}{\Delta x}[\mathbf{F}^{-}_{i+1/2} - \mathbf{F}^{+}_{i-1/2}] + \frac{\Delta t}{\Delta x}[\bar{\mathbf{S}}_{i_R, i_L}]\,, \tag{41}$$

with the numerical fluxes $\mathbf{F}^{-}_{i+1/2}$ and $\mathbf{F}^{+}_{i-1/2}$ as defined in (25). Adopting the flux-expansion ADER approach, we seek a truncated Taylor time expansion of the fluxes at the interfaces, as expressed in equation (40).

The Augmented version of the Roe solver [22] presented in [14, 25] is used here to solve the conventional RPs that appear when using the FS and LFS solvers. The ARoe solver takes into account the contribution of the source term in the solution, ensuring an exact balance between numerical fluxes and source terms.

In what follows, $\delta(\cdot)_{i+1/2}$ operator will represent the difference between the right and left state of the DRP centered in $i+1/2$ for a given variable, as $\delta(\cdot)_{i+1/2} = (\cdot)_{(i+1)_L} - (\cdot)_{i_R}$ and $\delta(\cdot)_{i-1/2} = (\cdot)_{i_L} - (\cdot)_{(i-1)_R}$. The ARoe solver is based on the decomposition of the approximate Jacobian of the homogeneous part at the initial time $\tilde{\mathbf{J}}_{i+1/2}(\mathbf{U}^{(0)}_{i_R}, \mathbf{U}^{(0)}_{(i+1)_L})$

$$\delta\mathbf{F}^{(0)}_{i+1/2} = \widetilde{\mathbf{J}}_{i+1/2}\delta\mathbf{U}^{(0)}_{i+1/2}\,, \tag{42}$$

leading to a set of approximated eigenvalues $\tilde{\lambda}^m_{i+1/2}$ and eigenvectors $\widetilde{\mathbf{e}}^m_{i+1/2} = (e^m_1, ..., e^m_{N_\lambda})^T$. The approximate Jacobian $\widetilde{\mathbf{J}}_{i+1/2}$ can be expressed as

$$\widetilde{\mathbf{J}}_{i+1/2} = \widetilde{\mathbf{P}}_{i+1/2}\mathbf{\Lambda}_{i+1/2}\widetilde{\mathbf{P}}^{-1}_{i+1/2}\,, \tag{43}$$

with $\widetilde{\mathbf{P}}_{i+1/2} = \left(\widetilde{\mathbf{e}}^1, ..., \widetilde{\mathbf{e}}^{N_\lambda}\right)_{i+1/2}$ an invertible matrix composed by the eigenvectors of $\widetilde{\mathbf{J}}_{i+1/2}$ and $\mathbf{\Lambda}_{i+1/2}$ the diagonal matrix composed by the eigenvalues of $\widetilde{\mathbf{J}}_{i+1/2}$.

The leading terms of the expansion in (40) are computed by solving the DRP_0, given by equation (35). When using the ARoe solver, the solution of the DRP_0 for the fluxes reads

$$\begin{aligned}
\mathbf{F}^{-,(0)}_{i_R} &= \mathbf{F}^{(0)}_{i_R} + \textstyle\sum_{m=1}^{N_\lambda}\left(\widetilde{\lambda}^{-}\alpha^{(0)} - \beta^{-,(0)}\right)^m_{i+1/2}\widetilde{\mathbf{e}}^m_{i+1/2}\,,\\
\mathbf{F}^{+,(0)}_{(i+1)_L} &= \mathbf{F}^{(0)}_{(i+1)_L} - \textstyle\sum_{m=1}^{N_\lambda}\left(\widetilde{\lambda}^{+}\alpha^{(0)} - \beta^{+,(0)}\right)^m_{i+1/2}\widetilde{\mathbf{e}}^m_{i+1/2}\,,
\end{aligned} \tag{44}$$

with $\mathbf{F}^{(0)}_{i_R}$ and $\mathbf{F}^{(0)}_{(i+1)_L}$ the physical fluxes defined in (14),

$$\left(\tilde{\lambda}^{\pm}\right)^m_{i+1/2} = \left(\frac{\widetilde{\lambda} \pm |\widetilde{\lambda}|}{2}\right)^m_{i+1/2}\,, \qquad \left(\beta^{\pm,(0)}\right)^m_{i+1/2} = \left(\frac{\widetilde{\lambda}^{\pm}}{\widetilde{\lambda}}\beta^{(0)}\right)^m_{i+1/2}\,, \tag{45}$$

$\alpha^{(0)}$ the wave strengths given by the projection of $\delta\mathbf{U}^{(0)}_{i+1/2}$ onto the Jacobian eigenvectors basis as

$$\delta\mathbf{U}^{(0)}_{i+1/2} = \widetilde{\mathbf{P}}_{i+1/2}\mathbf{A}_{i+1/2}\,, \tag{46}$$

with $\mathbf{A}_{i+1/2} = \left(\alpha^{(0),1}, ..., \alpha^{(0),N_\lambda}\right)^T_{i+1/2}$ and $\beta^{(0)}$ the source strengths associated to each wave, given by

$$\bar{\mathbf{S}}^{0}_{i+1/2} = \widetilde{\mathbf{P}}_{i+1/2}\mathbf{B}^{(0)}_{i+1/2}\,, \tag{47}$$

with $\mathbf{B}^{(0)}_{i+1/2} = \left(\beta^{(0),1},...,\beta^{(0),N_\lambda}\right)^T_{i+1/2}$. As in the scalar case, a suitable approximation of the integral of the source term across the interface

$$\bar{\mathbf{S}}^{(0)}_{i+1/2} = \frac{1}{\Delta t}\int_0^{\Delta t}\int_{x^-_{i+1/2}}^{x^+_{i+1/2}} \mathbf{S}(x,0)\;dx\;dt\,, \tag{48}$$

must be found when dealing with geometric source terms.

The same procedure is extended to derive the expression of the derivative terms of the numerical fluxes in (40). This is performed by solving the K RPs associated to the high order terms of the DRP$_K$, given by (36).

It is work mentioning that the numerical solution for these RPs is computed using an extension of the ARoe solver that does not use derivatives of the conserved variables, $\mathbf{D}^{(k)}_{i_R}$ and $\mathbf{D}^{(k)}_{(i+1)_L}$, as initial condition but derivatives of the fluxes at the interfaces instead, namely $\mathbf{R}^{(k)}_{i_R}$ and $\mathbf{R}^{(k)}_{(i+1)_L}$, according to the FS solver. The proposed solution provides the following approximate fluxes at the interface

$$\begin{aligned}
\mathbf{F}^{-,(k)}_{i_R} &= \mathbf{R}^{(k)}_{i_R} + \textstyle\sum_{m=1}^{N_\lambda}\left(\gamma^{-,(k)} - \beta^{-,(k)}\right)^m_{i+1/2}\widetilde{\mathbf{e}}^m_{i+1/2}\,,\\
\mathbf{F}^{+,(k)}_{(i+1)_L} &= \mathbf{R}^{(k)}_{(i+1)_L} - \textstyle\sum_{m=1}^{N_\lambda}\left(\gamma^{+,(k)} - \beta^{+,(k)}\right)^m_{i+1/2}\widetilde{\mathbf{e}}^m_{i+1/2}\,,
\end{aligned} \tag{49}$$

with

$$\left(\gamma^{\pm,(k)}\right)^m_{i+1/2} = \left(\frac{\widetilde{\lambda}^{\pm}}{\widetilde{\lambda}}\gamma^{(k)}\right)^m_{i+1/2}, \qquad \left(\beta^{\pm,(k)}\right)^m_{i+1/2} = \left(\frac{\widetilde{\lambda}^{\pm}}{\widetilde{\lambda}}\beta^{(k)}\right)^m_{i+1/2}. \tag{50}$$

The flux strengths, $\gamma^{(k)}$, are given in this case by the projection of the variation of $\mathbf{R}^{(k)}$ onto the Jacobian eigenvectors basis

$$\delta\mathbf{R}^{(k)}_{i+1/2} = \widetilde{\mathbf{P}}_{i+1/2}\mathbf{\Gamma}^{(k)}_{i+1/2}\,, \tag{51}$$

with $\mathbf{\Gamma}^{(k)}_{i+1/2} = \left(\gamma^{(k),1},...,\gamma^{(k),N_\lambda}\right)^T_{i+1/2}$, and the same for the source strengths, $\beta^{(k)}$, associated to each wave

$$\bar{\mathbf{S}}^{(k)}_{i+1/2} = \widetilde{\mathbf{P}}_{i+1/2}\mathbf{B}^{(k)}_{i+1/2}\,, \tag{52}$$

with $\mathbf{B}^{(k)}_{i+1/2} = \left(\beta^{(k),1},...,\beta^{(k),N_\lambda}\right)^T_{i+1/2}$. A suitable approximation of the integral of the source term across the interface

$$\bar{\mathbf{S}}^{(k)}_{i+1/2} = \frac{1}{\Delta t}\int_0^{\Delta t}\int_{x^-_{i+1/2}}^{x^+_{i+1/2}} \mathbf{Q}^{(k)}\; dx\; dt\,, \tag{53}$$

must be found when dealing with geometric source terms.

Recall that the centered contribution of the source term, $\bar{\mathbf{S}}_{i_R,i_L}$, is included in the updating scheme (41). It is expressed as a leading term plus K additional higher order terms

$$\bar{\mathbf{S}}_{i_R,i_L} = \bar{\mathbf{S}}^{(0)}_{i_R,i_L} + \sum_{k=1}^{K}\bar{\mathbf{S}}^{(k)}_{i_R,i_L}\,, \tag{54}$$

with

$$\bar{\mathbf{S}}^{(0)}_{i_R,i_L} = \frac{1}{\Delta t}\int_0^{\Delta t}\int_{x_{i-1/2}}^{x_{i+1/2}} \mathbf{S}_i(x,0)\; dx\; dt\,, \tag{55}$$

$$\bar{\mathbf{S}}^{(k)}_{i_R,i_L} = \frac{1}{\Delta t}\int_0^{\Delta t}\int_{x_{i-1/2}}^{x_{i+1/2}} \mathbf{Q}^{(k)}\frac{\tau^k}{k!}\; dx\; dt\,, \tag{56}$$

computed by suitable approximations of the integrals.

As outlined in previous sections, $\delta\mathbf{M}^+_{i-1/2}$ and $\delta\mathbf{M}^-_{i+1/2}$ represent the contributions of the incoming waves at cell interfaces and are expressed as

$$\delta\mathbf{M}^{+,(0)}_{i-1/2} = \sum_{m=1}^{N_\lambda}\left[\left(\widetilde{\lambda}^+\alpha^{(0)} - \beta^{+,(0)}\right)\widetilde{\mathbf{e}}\right]^m_{i-1/2}\,, \tag{57}$$

$$\delta\mathbf{M}^{+,(k)}_{i-1/2} = \sum_{k=1}^{K}\sum_{m=1}^{N_\lambda}\left(\left(\gamma^{+,(k)} - \beta^{+,(k)}\right)\widetilde{\mathbf{e}}\right)^m_{i-1/2}\frac{\Delta t^k}{(k+1)!}\,, \tag{58}$$

$$\delta\mathbf{M}^{-,(0)}_{i+1/2} = \sum_{m=1}^{N_\lambda}\left[\left(\widetilde{\lambda}^-\alpha^{(0)} - \beta^{-,(0)}\right)\widetilde{\mathbf{e}}\right]^m_{i+1/2}\,, \tag{59}$$

$$\delta\mathbf{M}^{-,(k)}_{i+1/2} = \sum_{k=1}^{K}\sum_{m=1}^{N_\lambda}\left(\left(\gamma^{-,(k)}-\beta^{-,(k)}\right)\widetilde{\mathbf{e}}\right)^m_{i+1/2}\frac{\Delta t^k}{(k+1)!} \tag{60}$$

and $\delta\mathbf{M}_{i_R,i_L}$ accounts for both the variation of the physical fluxes and the contribution of the source term inside the cell

$$\begin{aligned}\delta\mathbf{M}_{i_R,i_L} &= \bar{\mathbf{F}}_{i_R} - \bar{\mathbf{F}}_{i_L} - \bar{\mathbf{S}}_{i_R,i_L} = \\ &= \left(\mathbf{F}^{(0)}_{i_R} + \sum_{k=1}^{K}\mathbf{R}^{(k)}_{i_R}\frac{\Delta t^k}{(k+1)!}\right) - \left(\mathbf{F}^{(0)}_{i_L} + \sum_{k=1}^{K}\mathbf{R}^{(k)}_{i_L}\frac{\Delta t^k}{(k+1)!}\right) - \bar{\mathbf{S}}_{i_R,i_L}\,.\end{aligned} \tag{61}$$

4.1. Linear approach for the high order terms: The ARL-ADER scheme.

When using the LFS Derivative Riemann solver, RPs for the derivatives are given by (37) instead of (36). The numerical solution for (37) is computed using an extension of the ARoe solver that, in this case, only uses derivatives of the conserved variables, $\mathbf{D}^{(k)}_{i_R}$ and $\mathbf{D}^{(k)}_{(i+1)_L}$, as initial condition. The proposed solution for the approximate derivative fluxes at the interfaces is

$$\begin{aligned}\mathbf{F}^{-,(k)}_{i_R} &= \widetilde{\mathbf{J}}_{i+1/2}\mathbf{D}^{(k)}_{i_R} + \textstyle\sum_{m=1}^{N_\lambda}\left(\widetilde{\lambda}^-\alpha^{(k)} - \beta^{-,(k)}\right)^m_{i+1/2}\widetilde{\mathbf{e}}^m_{i+1/2}\,,\\ \mathbf{F}^{+,(k)}_{(i+1)_L} &= \widetilde{\mathbf{J}}_{i+1/2}\mathbf{D}^{(k)}_{(i+1)_L} - \textstyle\sum_{m=1}^{N_\lambda}\left(\widetilde{\lambda}^+\alpha^{(k)} - \beta^{+,(k)}\right)^m_{i+1/2}\widetilde{\mathbf{e}}^m_{i+1/2}\,,\end{aligned} \tag{62}$$

with

$$\left(\tilde{\lambda}^{\pm}\right)^m_{i+1/2} = \left(\frac{\widetilde{\lambda}\pm|\widetilde{\lambda}|}{2}\right)^m_{i+1/2}, \qquad \left(\beta^{\pm,(0)}\right)^m_{i+1/2} = \left(\frac{\widetilde{\lambda}^{\pm}}{\widetilde{\lambda}}\beta^{(0)}\right)^m_{i+1/2}. \tag{63}$$

The wave strengths, $\alpha^{(k)}$, are given in this case by the projection of the jump of $\mathbf{D}^{(k)}$ onto the Jacobian eigenvectors basis

$$\delta\mathbf{D}^{(k)}_{i+1/2} = \widetilde{\mathbf{P}}_{i+1/2}\mathbf{A}^{(k)}_{i+1/2}\,, \tag{64}$$

with $\mathbf{A}_{i+1/2}^{(k)} = \left(\alpha^{(k),1}, ..., \alpha^{(k),N_\lambda}\right)_{i+1/2}^{T}$. The source strengths, $\beta^{(k)}$, associated to each wave are computed as proposed in the original approach, using (52).

Contributions of the incoming waves at cell interfaces, $\delta\mathbf{M}_{i-1/2}^{+}$ and $\delta\mathbf{M}_{i+1/2}^{-}$, will be now expressed as

$$\delta\mathbf{M}_{i-1/2}^{+,(0)} = \sum_{m=1}^{N_\lambda} \left[\left(\widetilde{\lambda}^{+} \alpha^{(0)} - \beta^{+,(0)} \right) \widetilde{\mathbf{e}} \right]_{i-1/2}^{m} , \tag{65}$$

$$\delta\mathbf{M}_{i-1/2}^{+,(k)} = \sum_{k=1}^{K} \sum_{m=1}^{N_\lambda} \left(\left(\widetilde{\lambda}^{-} \alpha^{(k)} - \beta^{+,(k)} \right) \widetilde{\mathbf{e}} \right)_{i-1/2}^{m} \frac{\Delta t^k}{(k+1)!} , \tag{66}$$

$$\delta\mathbf{M}_{i+1/2}^{-,(0)} = \sum_{m=1}^{N_\lambda} \left[\left(\widetilde{\lambda}^{-} \alpha^{(0)} - \beta^{-,(0)} \right) \widetilde{\mathbf{e}} \right]_{i+1/2}^{m} , \tag{67}$$

$$\delta\mathbf{M}_{i+1/2}^{-,(k)} = \sum_{k=1}^{K} \sum_{m=1}^{N_\lambda} \left(\left(\widetilde{\lambda}^{+} \alpha^{(k)} - \beta^{-,(k)} \right) \widetilde{\mathbf{e}} \right)_{i+1/2}^{m} \frac{\Delta t^k}{(k+1)!} , \tag{68}$$

while the centered fluctuation is calculated as in (61).

5. The HLLS-ADER scheme

In the framework of first order Godunov's method, Harten, Lax and van Leer introduced a novel Riemann solver [23], called HLL solver. This solver was of application for homogeneous RPs of two waves, providing an estimation of the intercell numerical flux considering a single star region. Such flux is directly computed from the integral form of the governing equations. When dealing with non-homogeneous systems of PDEs, the HLL solver can not be used. A proper treatment of source terms in the framework of the HLL solver was proposed by Murillo in [25] with the generation of a new solver, called HLLS, that considers the presence of an additional stationary wave at $x = 0$. In this section, the HLLS solver presented in [25] is extended for the resolution of the DRP by means of the FS solver and LFS solver, allowing to construct an ADER type numerical scheme.

The flux-expansion methodology is also used here, hence numerical fluxes will be calculated as the power series expansion in (40). This means that, as done in the AR-ADER scheme, the resolution of the DRP is done by solving the $K + 1$ RPs associated to the leading term and the derivatives. To this end, the HLLS solver [25] is used for the computation of the leading term,

whereas two different approaches are proposed for the computation of the high order terms: the first option is to use the HLLS solver for the nonlinear evolution equations associated to the derivatives and the second option is to linearize those equations and use the HLLS solver to obtain the solution. It is worth mentioning that the HLLS solver is a nonlinear Riemann solver unlike the ARoe solver but it can also be used to provide the solution of linear RPs with source term. In addition to this, it is remarkable to say that the HLLS solver contains in its structure the full set of waves present in the exact solution of the RP.

We depart from the original DRP in (11) considering for this derivation that $\mathbf{U}(x,t) \in \mathcal{C} \subseteq \mathbb{R}^2$ and $\mathbf{F}(\mathbf{U}) : \mathcal{C} \to \mathbb{R}^2$, that is, (11) is a system of two equations characterized by two real eigenvalues $\lambda^1(\mathbf{U}) \leq \lambda^2(\mathbf{U})$ corresponding to the wave speeds plus an extra wave of speed $\mathcal{S} = 0$ at $x = 0$.

The leading terms, $\mathbf{F}^{-,0}_{i_R}$ and $\mathbf{F}^{+,0}_{(i+1)_L}$, are calculated by solving the so-called DRP_0, corresponding to RP in (35)and depicted in Figure 4.

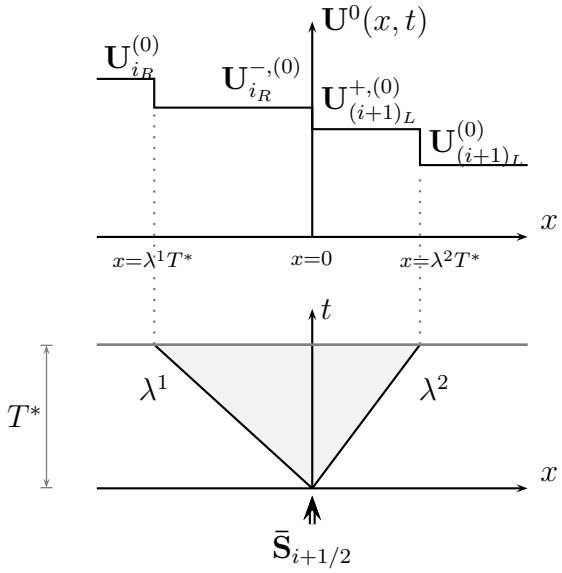

Figure 4: Values of the solution for the DRP_0, $\mathbf{U}^0(x,t)$, in each wedge of the (x,t) plane.

The integral form of (35) inside a control volume $[-x_L, x_R] \times [0, T^*]$ provides the expression for the integral volume of $\mathbf{U}(x,T^*)$ as

$$\int_{-x_L}^{x_R} \mathbf{U}(x,T^*)\,dx = x_R \mathbf{U}^{(0)}_{(i+1)_L} + x_L \mathbf{U}^{(0)}_{i_R} + (\mathbf{F}^{(0)}_{i_R} - \mathbf{F}^{(0)}_{(i+1)_L})T^* + \bar{\mathbf{S}}^{(0)}_{i+\frac{1}{2}} T^*\,, \quad (69)$$

with conserved quantities, fluxes and source as defined in Section 2. The integral on the left hand side of (69) can be split considering a wave structure given by $\lambda^1 \leq 0 \leq \lambda^2$ as depicted in Figure 4 and with $-x_L < \lambda^1 T^*$ and $x_R > \lambda^2 T^*$

$$\begin{aligned}\int_{-x_L}^{x_R} \mathbf{U}(x,T^*)\,dx = & \int_{-x_L}^{\lambda^1 T^*} \mathbf{U}(x,T^*)\,dx + \int_{\lambda^1 T^*}^{0} \mathbf{U}(x,T^*)\,dx + \\ & \int_{0}^{\lambda^2 T^*} \mathbf{U}(x,T^*)\,dx + \int_{\lambda^2 T^*}^{x_R} \mathbf{U}(x,T^*)\,dx\end{aligned} \quad (70)$$

and considering the solution composed of four constant states as shown in Figure 4, it yields

$$\begin{aligned}\int_{-x_L}^{x_R} \mathbf{U}(x,T^*)\,dx = & \mathbf{U}^{(0)}_{i_R}(\lambda^1 T^* + x_L) + \mathbf{U}^{(0)}_{(i+1)_L}(x_R - \lambda^2 T^*) + \\ & \mathbf{U}^{-,(0)}_{i_R}(-\lambda^1 T^*) + \mathbf{U}^{+,(0)}_{(i+1)_L}(\lambda^2 T^*)\,.\end{aligned} \quad (71)$$

Now, substitution of (71) in (69) leads to

$$(\mathbf{U}^{(0)}_{i_R} - \mathbf{U}^{-,(0)}_{i_R})\lambda^1 - (\mathbf{U}^{(0)}_{(i+1)_L} - \mathbf{U}^{+,(0)}_{(i+1)_L})\lambda^2 + \mathbf{F}^{(0)}_{(i+1)_L} - \mathbf{F}^{(0)}_{i_R} = \bar{\mathbf{S}}^{(0)}_{i+\frac{1}{2}}\,, \quad (72)$$

where an extra condition is needed in order to obtain an expression for $\mathbf{U}^{-,(0)}_{i_R}$ and $\mathbf{U}^{+,(0)}_{(i+1)_L}$, due to the presence of the source term. For that purpose, let us define first an approximate flux function $\hat{\mathbf{F}}(x,t)$ with a similar structure than $\mathbf{U}(x,t)$ as depicted in Figure 4. In this case, also intercell values for the fluxes can be defined at both sides of the t axis as

$$\mathbf{F}^{-,(0)}_{i_R} = \lim_{x\to 0^-} \hat{\mathbf{F}}(x,t)\,, \qquad \mathbf{F}^{+,(0)}_{(i+1)_L} = \lim_{x\to 0^+} \hat{\mathbf{F}}(x,t)\,. \quad (73)$$

The following RH relations across waves between fluxes and conserved variables are stated

$$\mathbf{F}_{i_R}^{-,(0)} - \mathbf{F}_{i_R}^{(0)} = \lambda^1(\mathbf{U}_{i_R}^{-,(0)} - \mathbf{U}_{i_R}^{(0)})\,, \tag{74}$$

$$\mathbf{F}_{(i+1)_L}^{(0)} - \mathbf{F}_{(i+1)_L}^{+,(0)} = \lambda^2(\mathbf{U}_{(i+1)_L}^{(0)} - \mathbf{U}_{(i+1)_L}^{+,(0)})\,, \tag{75}$$

$$\mathbf{F}_{(i+1)_L}^{+,(0)} - \mathbf{F}_{i_R}^{-,(0)} - \bar{\mathbf{S}}_{i+\frac{1}{2}}^{(0)} = \mathcal{S}(\mathbf{U}_{(i+1)_L}^{+,(0)} - \mathbf{U}_{i_R}^{-,(0)}) = 0\,. \tag{76}$$

Moreover, using Roe's approach it is possible to define the following relation as done in the derivation of the AR-ADER scheme

$$\mathbf{F}_{(i+1)_L}^{+,(0)} - \mathbf{F}_{i_R}^{-,(0)} = \widetilde{\mathbf{J}}_{i+\frac{1}{2}} \left(\mathbf{U}_{(i+1)_L}^{+,(0)} - \mathbf{U}_{i_R}^{-,(0)} \right)\,, \tag{77}$$

where $\widetilde{\mathbf{J}}_{i+\frac{1}{2}} = \widetilde{\mathbf{J}}_{i+\frac{1}{2}}(\mathbf{U}_{i_R}^{-,(0)}, \mathbf{U}_{(i+1)_L}^{+,(0)})$ is an approximation of the Jacobian matrix according to equations (42) and (43). Combining (76) and (77), the following relation appears

$$\bar{\mathbf{S}}_{i+\frac{1}{2}}^{(0)} = \widetilde{\mathbf{J}}_{i+\frac{1}{2}} \left(\mathbf{U}_{(i+1)_L}^{+,(0)} - \mathbf{U}_{i_R}^{-,(0)} \right)\,, \tag{78}$$

being possible to write the jump on the conserved variables across the stationary wave at $x = 0$ as

$$\mathbf{U}_{(i+1)_L}^{+,(0)} - \mathbf{U}_{i_R}^{-,(0)} = (\widetilde{\mathbf{P}}\widetilde{\mathbf{\Lambda}}^{-1}\widetilde{\mathbf{P}}^{-1})_{i+\frac{1}{2}} \bar{\mathbf{S}}_{i+\frac{1}{2}}^{(0)} = \bar{\mathbf{H}}_{i+\frac{1}{2}}^{(0)}\,. \tag{79}$$

Combination of (72) and (79) leads to the following values for the intermediate states

$$\mathbf{U}_{i_R}^{-,(0)} = \frac{\mathbf{F}_{i_R}^{(0)} - \mathbf{F}_{(i+1)_L}^{(0)} + \lambda^2 \mathbf{U}_{(i+1)_L}^{(0)} - \lambda^1 \mathbf{U}_{i_R}^{(0)} + \bar{\mathbf{S}}_{i+\frac{1}{2}}^{(0)} - \lambda^2 \bar{\mathbf{H}}_{i+\frac{1}{2}}^{(0)}}{\lambda^2 - \lambda^1}\,, \tag{80}$$

$$\mathbf{U}_{(i+1)_L}^{+,(0)} = \frac{\mathbf{F}_{i_R}^{(0)} - \mathbf{F}_{(i+1)_L}^{(0)} + \lambda^2 \mathbf{U}_{(i+1)_L}^{(0)} - \lambda^1 \mathbf{U}_{i_R}^{(0)} + \bar{\mathbf{S}}_{i+\frac{1}{2}}^{(0)} - \lambda^1 \bar{\mathbf{H}}_{i+\frac{1}{2}}^{(0)}}{\lambda^2 - \lambda^1}\,. \tag{81}$$

Remark that when the contribution of the source term is nil, relation in (79) shows that there only exists a unique intermediate state in the so-called star region. This state can be derived either from (80) or (81) indistinctly as

$$\mathbf{U}^* = \frac{\mathbf{F}^{(0)}_{i_R} - \mathbf{F}^{(0)}_{(i+1)_L} + \lambda^2 \mathbf{U}^{(0)}_{(i+1)_L} - \lambda^1 \mathbf{U}^{(0)}_{i_R}}{\lambda^2 - \lambda^1} \,. \tag{82}$$

Application of the RH conditions in (74) - (76) allows to calculate the expression for the zero-th order intercell fluxes. For this calculation, we will consider $\lambda^1 \leq 0 \leq \lambda^2$, that is, subcritical regime, and the approximate fluxes at both sides of the interface will be denoted by $\mathbf{F}^{-,(0),sub}_{i_R}$ and $\mathbf{F}^{+,(0),sub}_{(i+1)_L}$. Such fluxes read

$$\mathbf{F}^{-,(0),sub}_{i_R} = \frac{\lambda^2 \mathbf{F}^{(0)}_{i_R} - \lambda^1 \mathbf{F}^{(0)}_{(i+1)_L} + \lambda^1 \lambda^2 \delta \mathbf{U}^{(0)}_{i+\frac{1}{2}} + \lambda^1 \left(\bar{\mathbf{S}}^{(0)}_{i+\frac{1}{2}} - \lambda^2 \bar{\mathbf{H}}^{(0)}_{i+\frac{1}{2}} \right)}{\lambda^2 - \lambda^1} \,, \tag{83}$$

$$\mathbf{F}^{+,(0),sub}_{(i+1)_L} = \frac{\lambda^2 \mathbf{F}^{(0)}_{i_R} - \lambda^1 \mathbf{F}^{(0)}_{(i+1)_L} + \lambda^1 \lambda^2 \delta \mathbf{U}^{(0)}_{i+\frac{1}{2}} + \lambda^2 \left(\bar{\mathbf{S}}^{(0)}_{i+\frac{1}{2}} - \lambda^1 \bar{\mathbf{H}}^{(0)}_{i+\frac{1}{2}} \right)}{\lambda^2 - \lambda^1} \,. \tag{84}$$

with $\mathbf{F}^{(0)}_{i_R}$ and $\mathbf{F}^{(0)}_{(i+1)_L}$ the physical fluxes evaluated at both sides of the interface according to equation (14), $\mathbf{U}^{(0)}_{i_R}$ and $\mathbf{U}^{(0)}_{(i+1)_L}$ the reconstructed variables at both sides of the interface according to (12) and $\bar{\mathbf{S}}^{(0)}_{i+\frac{1}{2}}$ a suitable approximation of the integral of the sources across the interface according to (34).

When considering all different combinations of wave speeds, that is, not only the subcritical case considered above but also supercritical regimes, the general expression for the zero-th order intercell numerical fluxes reads

$$\mathbf{F}^{-,(0)}_{i_R} = \begin{cases} \mathbf{F}^{(0)}_{i_R} & \text{if} \quad \lambda^1 \geq 0 \\ \mathbf{F}^{-,(0),sub}_{i_R} & \text{if} \quad \lambda^1 \leq 0 \leq \lambda^2 \\ \mathbf{F}^{(0)}_{(i+1)_L} - \bar{\mathbf{S}}^{(0)}_{i+\frac{1}{2}} & \text{if} \quad \lambda^2 \leq 0 \end{cases} \,, \tag{85}$$

$$\mathbf{F}^{+,(0)}_{(i+1)_L} = \begin{cases} \mathbf{F}^{(0)}_{i_R} + \bar{\mathbf{S}}^{(0)}_{i+\frac{1}{2}} & \text{if} \quad \lambda^1 \geq 0 \\ \mathbf{F}^{+,(0),sub}_{(i+1)_L} & \text{if} \quad \lambda^1 \leq 0 \leq \lambda^2 \\ \mathbf{F}^{(0)}_{(i+1)_L} & \text{if} \quad \lambda^2 \leq 0 \end{cases} \,. \tag{86}$$

Terms associated to temporal derivatives of the fluxes in (40), $\mathbf{F}^{-,(k)}_{i_R}$ and $\mathbf{F}^{+,(k)}_{(i+1)_L}$, are calculated by solving the corresponding k-th order RPs in (36).

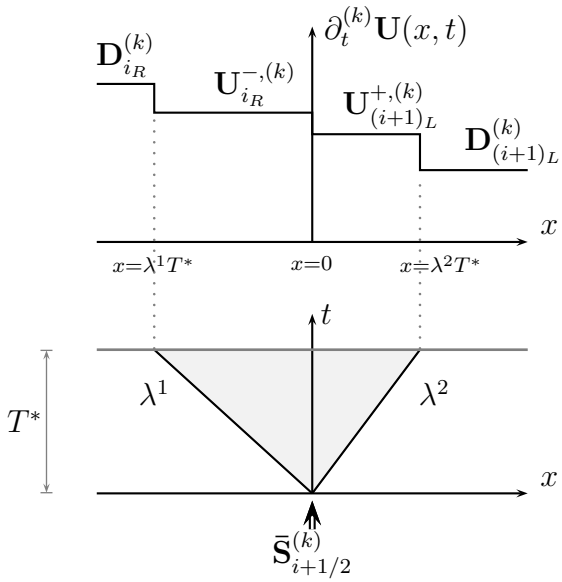

Figure 5: Values of the solution for the k-th order RP, $\partial_t \mathbf{U}^{(k)}(x,t)$, in each wedge of the (x,t) plane.

The integral form of (36) inside a control volume $[-x_L, x_R] \times [0, T^*]$ is expressed as

$$\int_{-x_L}^{x_R} \partial_t^{(k)} \mathbf{U}(x, T^*)\, dx = x_R \mathbf{D}_{(i+1)_L}^{(k)} + x_L \mathbf{D}_{i_R}^{(k)} + (\mathbf{R}_{i_R}^{(k)} - \mathbf{R}_{(i+1)_L}^{(k)}) T^* + \bar{\mathbf{S}}_{i+\frac{1}{2}}^{(k)} T^* \,, \tag{87}$$

with $\mathbf{D}^{(k)}$ and $\mathbf{R}^{(k)}$ properly defined in (21) and (19) respectively and the source term integrated as described in (34), when necessary. The integral on the left hand side of (69) can be split considering a wave structure given by $\lambda^1 \leq 0 \leq \lambda^2$ and with $-x_L < \lambda^1 T^*$ and $x_R > \lambda^2 T^*$ and considering the solution composed of four constant states as shown in Figure 5, it yields

$$\begin{aligned} \int_{-x_L}^{x_R} \partial_t^{(k)} \mathbf{U}(x, T^*)\, dx = \; & \mathbf{D}_{i_R}^{(k)} (\lambda^1 T^* + x_L) + \mathbf{D}_{(i+1)_L}^{(k)} (x_R - \lambda^2 T^*) + \\ & \mathbf{U}_{i_R}^{-,(k)} (-\lambda^1 T^*) + \mathbf{U}_{(i+1)_L}^{+,(k)} (\lambda^2 T^*) \,, \end{aligned} \tag{88}$$

where

$$\mathbf{U}_{i_R}^{-,(k)} = \lim_{x\to 0^-}\left[\partial_t^{(k)}\mathbf{U}(x,t)\right]_{t=T^*} \qquad \mathbf{U}_{(i+1)_L}^{+,(k)} = \lim_{x\to 0^+}\left[\partial_t^{(k)}\mathbf{U}(x,t)\right]_{t=T^*} \quad (89)$$

are the values of the solution for temporal derivatives at each side of the interface, as depicted in Figure 5. Notice that wave speeds λ^1 and λ^1 are considered constant and are yet to be defined.
Now, substitution of (88) in (87) leads to

$$\left(\mathbf{D}_{i_R}^{(k)} - \mathbf{U}_{i_R}^{-,(k)}\right)\lambda^1 - \left(\mathbf{D}_{(i+1)_L}^{(k)} - \mathbf{U}_{(i+1)_L}^{+,(k)}\right)\lambda^2 + \mathbf{R}_{(i+1)_L}^{(k)} - \mathbf{R}_{i_R}^{(k)} = \bar{\mathbf{S}}_{i+\frac{1}{2}}^{(k)}\,, \quad (90)$$

where an extra condition is needed in order to derive the expression for $\mathbf{U}_{i_R}^{-,(k)}$ and $\partial_t^{(k)}\mathbf{U}_{(i+1)_L}^{+}$, due to the presence of the source term. Before introducing this condition, let us define first an approximate function for the derivatives of the flux, denoted by $\partial_t^{(k)}\hat{\mathbf{F}}(x,t)$, with a similar structure than $\partial_t^{(k)}\mathbf{U}(x,t)$ as depicted in Figure 5. In this case, also intercell values for the fluxes can be defined at both sides of the t axis as

$$\mathbf{F}_{i_R}^{-,(k)} = \lim_{x\to 0^-}\left[\partial_t^{(k)}\hat{\mathbf{F}}(x,t)\right]_{t=T^*}, \qquad \mathbf{F}_{(i+1)_L}^{+,(k)} = \lim_{x\to 0^+}\left[\partial_t^{(k)}\hat{\mathbf{F}}(x,t)\right]_{t=T^*}. \quad (91)$$

For that purpose, the following RH relations across waves between derivatives of fluxes and conserved variables are stated

$$\mathbf{F}_{i_R}^{-,(k)} - \mathbf{R}_{i_R}^{(k)} = \lambda^1\left(\mathbf{U}_{i_R}^{-,(k)} - \mathbf{D}_{i_R}^{(k)}\right), \quad (92)$$

$$\mathbf{R}_{(i+1)_L}^{(k)} - \mathbf{F}_{(i+1)_L}^{+,(k)} = \lambda^2\left(\mathbf{D}_{(i+1)_L}^{(k)} - \mathbf{U}_{(i+1)_L}^{+,(k)}\right), \quad (93)$$

$$\mathbf{F}_{(i+1)_L}^{+,(k)} - \mathbf{F}_{i_R}^{-,(k)} - \bar{\mathbf{S}}_{i+\frac{1}{2}}^{(k)} = 0\,. \quad (94)$$

As mentioned before, velocities λ^1 and λ^2 were considered constant but have not been defined yet. The proposed approach is to assign the same velocities that those for the leading term, obtained from the approximate Jacobian evaluated at both sides of the discontinuity at $t=0$, $\widetilde{\mathbf{J}}_{i+\frac{1}{2}} = \widetilde{\mathbf{J}}(\mathbf{U}_{i_R}^{(0)}, \mathbf{U}_{(i+1)_L}^{(0)})$, using Roe's technique. Under this assumption, it is possible to derive the following relation from (77) as

$$\mathbf{F}^{+,(k)}_{(i+1)_L} - \mathbf{F}^{-,(k)}_{i_R} = \widetilde{\mathbf{J}}^{(0)}_{i+\frac{1}{2}} \left(\mathbf{U}^{+,(k)}_{(i+1)_L} - \mathbf{U}^{-,(k)}_{i_R} \right) , \tag{95}$$

since derivatives of the Jacobian matrix are neglected.
Combining (94) and (95), the following relation appears

$$\bar{\mathbf{S}}^{(k)}_{i+\frac{1}{2}} = \widetilde{\mathbf{J}}^{(0)}_{i+\frac{1}{2}} \left(\mathbf{U}^{+,(k)}_{(i+1)_L} - \mathbf{U}^{-,(k)}_{i_R} \right) \tag{96}$$

and using (43), it is possible to write the jump on the conserved variables across the stationary wave at $x = 0$ as

$$\mathbf{U}^{+,(k)}_{(i+1)_L} - \mathbf{U}^{-,(k)}_{i_R} = (\widetilde{\mathbf{P}} \widetilde{\mathbf{\Lambda}}^{-1} \widetilde{\mathbf{P}}^{-1})_{i+\frac{1}{2}} \bar{\mathbf{S}}^{(k)}_{i+\frac{1}{2}} = \bar{\mathbf{H}}^{(k)}_{i+\frac{1}{2}} , \tag{97}$$

where $\widetilde{\mathbf{P}}$ is a matrix composed by the eigenvectors of the Jacobian that leads to the following diagonalization

$$\widetilde{\mathbf{J}}^{(0)}_{i+\frac{1}{2}} = (\widetilde{\mathbf{P}} \widetilde{\mathbf{\Lambda}} \widetilde{\mathbf{P}}^{-1})_{i+\frac{1}{2}} , \tag{98}$$

with $\widetilde{\mathbf{\Lambda}}$ a diagonal matrix composed by the eigenvalues of the Jacobian.

The expression for the intercell fluxes can be obtained by combining (97) with (90) and using the RH relations stated before

$$\mathbf{F}^{-,(k),sub}_{i_R} = \frac{\lambda^2 \mathbf{R}^{(k)}_{i_R} - \lambda^1 \mathbf{R}^{(k)}_{(i+1)_L} + \lambda^1 \lambda^2 \delta \mathbf{D}^{(k)}_{i+\frac{1}{2}} + \lambda^1 \left(\bar{\mathbf{S}}^{(k)}_{i+\frac{1}{2}} - \lambda^2 \bar{\mathbf{H}}^{(k)}_{i+\frac{1}{2}} \right)}{\lambda^2 - \lambda^1} , \tag{99}$$

$$\mathbf{F}^{+,(k),sub}_{(i+1)_L} = \frac{\lambda^2 \mathbf{R}^{(k)}_{i_R} - \lambda^1 \mathbf{R}^{(k)}_{(i+1)_L} + \lambda^1 \lambda^2 \delta \mathbf{D}^{(k)}_{i+\frac{1}{2}} + \lambda^2 \left(\bar{\mathbf{S}}^{(k)}_{i+\frac{1}{2}} - \lambda^1 \bar{\mathbf{H}}^{(k)}_{i+\frac{1}{2}} \right)}{\lambda^2 - \lambda^1} . \tag{100}$$

High order terms of the numerical fluxes in (40) are finally calculated using the following approximate flux that considers all possible wave structures

$$\mathbf{F}^{-,(k)}_{i_R} = \begin{cases} \mathbf{R}^{(k)}_{i_R} & \text{if} \quad \lambda^1 \geq 0 \\ \mathbf{F}^{-,(k),sub}_{i_R} & \text{if} \quad \lambda^1 \leq 0 \leq \lambda^2 \\ \mathbf{R}^{(k)}_{(i+1)_L} - \bar{\mathbf{S}}^{(k)}_{i+\frac{1}{2}} & \text{if} \quad \lambda^2 \leq 0 \end{cases} , \tag{101}$$

$$\mathbf{F}^{+,(k)}_{(i+1)_L} = \begin{cases} \mathbf{R}^{(k)}_{i_R} + \bar{\mathbf{S}}^{(k)}_{i+\frac{1}{2}} & \text{if} \quad \lambda^1 \geq 0 \\ \mathbf{F}^{+,(k),sub}_{(i+1)_L} & \text{if} \quad \lambda^1 \leq 0 \leq \lambda^2 \\ \mathbf{R}^{(k)}_{(i+1)_L} & \text{if} \quad \lambda^2 \leq 0 \end{cases} . \tag{102}$$

Godunov's updating scheme can also be expressed in terms of contributions, namely those corresponding to RPs at the interfaces plus the contribution due to the variations of the variables inside the cell.

Fluctuations corresponding to the interfaces are next presented. After some algebraic manipulation of the equations, the following expressions for the contributions associated to the right interface are obtained for $\lambda^1 \leq 0 \leq \lambda^2$

$$\delta\mathbf{M}^{-,(0),sub}_{i+\frac{1}{2}} = \frac{-\lambda^1\delta\mathbf{F}^{(0)}_{i+\frac{1}{2}} + \lambda^1\lambda^2\delta\mathbf{U}^{(0)}_{i+\frac{1}{2}} + \lambda^1\left(\bar{\mathbf{S}}^{(0)}_{i+\frac{1}{2}} - \lambda^2\bar{\mathbf{H}}^{(0)}_{i+\frac{1}{2}}\right)}{\lambda^2 - \lambda^1},$$

$$\delta\mathbf{M}^{-,(k),sub}_{i+\frac{1}{2}} = \left[\frac{-\lambda^1\delta\mathbf{R}^{(k)}_{i+\frac{1}{2}} + \lambda^1\lambda^2\delta\mathbf{D}^{(k)}_{i+\frac{1}{2}} + \lambda^1\left(\bar{\mathbf{S}}^{(k)}_{i+\frac{1}{2}} - \lambda^2\bar{\mathbf{H}}^{(k)}_{i+\frac{1}{2}}\right)}{\lambda^2 - \lambda^1}\right]\frac{\Delta t^k}{(k+1)!}. \tag{103}$$

Expressions for the contributions associated to the left interface are presented next, for $\lambda^1 \leq 0 \leq \lambda^2$

$$\delta\mathbf{M}^{+,(0),sub}_{i-\frac{1}{2}} = -\frac{-\lambda^2\delta\mathbf{F}^{(0)}_{i-\frac{1}{2}} + \lambda^1\lambda^2\delta\mathbf{U}^{(0)}_{i-\frac{1}{2}} + \lambda^2\left(\bar{\mathbf{S}}^{(0)}_{i-\frac{1}{2}} - \lambda^1\bar{\mathbf{H}}^{(0)}_{i-\frac{1}{2}}\right)}{\lambda^2 - \lambda^1},$$

$$\delta\mathbf{M}^{+,(k),sub}_{i-\frac{1}{2}} = -\left[\frac{-\lambda^2\delta\mathbf{R}^{(k)}_{i-\frac{1}{2}} + \lambda^1\lambda^2\delta\mathbf{D}^{(k)}_{i-\frac{1}{2}} + \lambda^2\left(\bar{\mathbf{S}}^{(k)}_{i-\frac{1}{2}} - \lambda^1\bar{\mathbf{H}}^{(k)}_{i-\frac{1}{2}}\right)}{\lambda^2 - \lambda^1}\right]\frac{\Delta t^k}{(k+1)!}. \tag{104}$$

As done for the fluxes, all possible combinations of wave speeds must be considered. The previous expressions provide the incoming wave contributions under subcritical flow regime but we also need to consider supercritical flow, that is $\lambda^1 > 0$ or $\lambda^2 < 0$. The complete expression for the fluctuations at the interfaces reads

$$\delta\mathbf{M}^{-,(0)}_{i+1/2} = \begin{cases} 0 & \text{if} \quad \lambda^1 \geq 0 \\ \delta\mathbf{M}^{-,(0),sub}_{i+1/2} & \text{if} \quad \lambda^1 \leq 0 \leq \lambda^2 \\ \delta\mathbf{F}^{(0)}_{i+1/2} - \bar{\mathbf{S}}^{(0)}_{i+1/2} & \text{if} \quad \lambda^2 \leq 0 \end{cases}, \tag{105}$$

$$\delta\mathbf{M}^{-,(k)}_{i+1/2} = \begin{cases} 0 & \text{if} \quad \lambda^1 \geq 0 \\ \delta\mathbf{M}^{-,(k),sub}_{i+1/2} & \text{if} \quad \lambda^1 \leq 0 \leq \lambda^2 \\ \delta\mathbf{R}^{(k)}_{i+1/2}\frac{\Delta t^k}{(k+1)!} - \bar{\mathbf{S}}^{(k)}_{i+1/2} & \text{if} \quad \lambda^2 \leq 0 \end{cases}, \tag{106}$$

$$\delta\mathbf{M}^{+,(0)}_{i-1/2} = \begin{cases} \delta\mathbf{F}^{(0)}_{i-1/2} - \bar{\mathbf{S}}^{(0)}_{i-1/2} & \text{if} \quad \lambda^1 \geq 0 \\ \delta\mathbf{M}^{+,(0),sub}_{i-1/2} & \text{if} \quad \lambda^1 \leq 0 \leq \lambda^2 \\ 0 & \text{if} \quad \lambda^2 \leq 0 \end{cases}, \tag{107}$$

$$\delta\mathbf{M}^{+,(k)}_{i-1/2} = \begin{cases} \delta\mathbf{R}^{(k)}_{i-1/2}\frac{\Delta t^k}{(k+1)!} - \bar{\mathbf{S}}^{(k)}_{i-1/2} & \text{if} \quad \lambda^1 \geq 0 \\ \delta\mathbf{M}^{+,(k),sub}_{i-1/2} & \text{if} \quad \lambda^1 \leq 0 \leq \lambda^2 \\ 0 & \text{if} \quad \lambda^2 \leq 0 \end{cases}, \tag{108}$$

Under steady conditions, all contributions must become nil in order to preserve the equilibrium of the numerical solution and achieve the steady regime. A proper factorization of the equations provided by the Cauchy-Kowalevski procedure allows to express temporal derivatives as a sum of factors multiplied by spatial derivatives of certain variables that are constant in space under steady regime. In this way, all temporal derivatives are enforced to be zero in steady state and therefore it is possible to affirm

$$\delta\mathbf{M}^{(k)}_{i_R,i_L} = \delta\mathbf{M}^{-,(k)}_{i+1/2} = \delta\mathbf{M}^{+,(k)}_{i-1/2} = 0\,, \tag{109}$$

On the other hand, contributions associated to the leading term, $\delta\mathbf{M}^{+,(0)}_{i-1/2}$ and $\delta\mathbf{M}^{-,(0)}_{i+1/2}$, will become zero if a proper equilibrium between sources and fluxes is guaranteed.

5.1. Linear approach for the high order terms: The HLLSL-ADER scheme.

When using the LFS method, RPs corresponding to the linearized equations of evolution for the derivatives must be computed. The resolution of such problems using the HLLS solver is addressed in this section. The LFS Derivative Riemann solver is constructed now in combination with the HLLS

solver. Recall that this strategy only requires the reconstruction of time derivatives of the conserved quantities at the interfaces, unlike the previous approach that also requires time derivatives of the fluxes.

The integral form of (37) inside a control volume $[-x_L, x_R] \times [0, T^*]$ is expressed as

$$\int_{-x_L}^{x_R} \partial_t^{(k)} \mathbf{U}(x, T^*)\, dx = x_R \mathbf{D}^{(k)}_{(i+1)_L} + x_L \mathbf{D}^{(k)}_{i_R} + \widetilde{\mathbf{J}}_{i+1/2}(\mathbf{D}^{(k)}_{i_R} - \mathbf{D}^{(k)}_{(i+1)_L}) T^* + \bar{\mathbf{S}}^{(k)}_{i+\frac{1}{2}} T^* \tag{110}$$

and the integral on the left hand side of (110) can be expressed as a sum of four constant states as done in (88). Substitution of (88) in (110) leads to an expression which is equivalent to (90) and reads

$$\left(\mathbf{D}^{(k)}_{i_R} - \mathbf{U}^{-,(k)}_{i_R}\right) \lambda^1 - \left(\mathbf{D}^{(k)}_{(i+1)_L} - \mathbf{U}^{+,(k)}_{(i+1)_L}\right) \lambda^2 + \widetilde{\mathbf{J}}_{i+1/2} \mathbf{D}^{(k)}_{(i+1)_L} - \widetilde{\mathbf{J}}_{i+1/2} \mathbf{D}^{(k)}_{i_R} = \bar{\mathbf{S}}^{(k)}_{i+\frac{1}{2}}\,. \tag{111}$$

As in the original case, an extra condition is needed in order to derive the expression for $\mathbf{U}^{-,(k)}_{i_R}$ and $\mathbf{U}^{+,(k)}_{(i+1)_L}$, due to the presence of the source term. Such condition was derived before and presented in equation (97).

The expression for the intercell fluxes, when $\lambda^1 \leq 0 \leq \lambda^2$, reads

$$\mathbf{F}^{-,(k),sub}_{i_R} = \frac{\widetilde{\mathbf{J}}_{i+1/2}\left(\lambda^2 \mathbf{D}^{(k)}_{i_R} - \lambda^1 \mathbf{D}^{(k)}_{(i+1)_L}\right) + \lambda^1 \lambda^2 \delta \mathbf{D}^{(k)}_{i+\frac{1}{2}} + \lambda^1 \left(\bar{\mathbf{S}}^{(k)}_{i+\frac{1}{2}} - \lambda^2 \bar{\mathbf{H}}^{(k)}_{i+\frac{1}{2}}\right)}{\lambda^2 - \lambda^1}\,, \tag{112}$$

$$\mathbf{F}^{+,(k),sub}_{(i+1)_L} = \frac{\widetilde{\mathbf{J}}_{i+1/2}\left(\lambda^2 \mathbf{D}^{(k)}_{i_R} - \lambda^1 \mathbf{D}^{(k)}_{(i+1)_L}\right) + \lambda^1 \lambda^2 \delta \mathbf{D}^{(k)}_{i+\frac{1}{2}} + \lambda^2 \left(\bar{\mathbf{S}}^{(k)}_{i+\frac{1}{2}} - \lambda^1 \bar{\mathbf{H}}^{(k)}_{i+\frac{1}{2}}\right)}{\lambda^2 - \lambda^1}\,. \tag{113}$$

The high order terms of the numerical fluxes in (40) are finally calculated using the following approximate flux that considers all possible wave structures

$$\mathbf{F}_{i_R}^{-,(k)} = \begin{cases} \widetilde{\mathbf{J}}_{i+1/2}\mathbf{D}_{i_R}^{(k)} & \text{if} \quad \lambda^1 \geq 0 \\ \mathbf{F}_{i_R}^{-,(k),sub} & \text{if} \quad \lambda^1 \leq 0 \leq \lambda^2 \\ \widetilde{\mathbf{J}}_{i+1/2}\mathbf{D}_{(i+1)_L}^{(k)} - \bar{\mathbf{S}}_{i+\frac{1}{2}}^{(k)} & \text{if} \quad \lambda^2 \leq 0 \end{cases}, \tag{114}$$

$$\mathbf{F}_{(i+1)_L}^{+,(k)} = \begin{cases} \widetilde{\mathbf{J}}_{i+1/2}\mathbf{D}_{i_R}^{(k)} + \bar{\mathbf{S}}_{i+\frac{1}{2}}^{(k)} & \text{if} \quad \lambda^1 \geq 0 \\ \mathbf{F}_{(i+1)_L}^{+,(k),sub} & \text{if} \quad \lambda^1 \leq 0 \leq \lambda^2 \\ \widetilde{\mathbf{J}}_{i+1/2}\mathbf{D}_{(i+1)_L}^{(k)} & \text{if} \quad \lambda^2 \leq 0 \end{cases}. \tag{115}$$

The high order contributions of the incoming waves at the interfaces when considering subcritical flow regime are computed as

$$\delta\mathbf{M}_{i+1/2}^{-,(k),sub} =$$

$$\left[\frac{-\lambda^1\widetilde{\mathbf{J}}_{i+1/2}\delta\mathbf{D}_{i+\frac{1}{2}}^{(k)} + \lambda^1\lambda^2\delta\mathbf{D}_{i+\frac{1}{2}}^{(k)} + \lambda^1\left(\bar{\mathbf{S}}_{i+\frac{1}{2}}^{(k)} - \lambda^2\bar{\mathbf{H}}_{i+\frac{1}{2}}^{(k)}\right)}{\lambda^2 - \lambda^1}\right]\frac{\Delta t^k}{(k+1)!}, \tag{116}$$

$$\delta\mathbf{M}_{i-1/2}^{+,(k),sub} =$$

$$-\left[\frac{-\lambda^2\widetilde{\mathbf{J}}_{i+1/2}\delta\mathbf{D}_{i-\frac{1}{2}}^{(k)} + \lambda^1\lambda^2\delta\mathbf{D}_{i-\frac{1}{2}}^{(k)} + \lambda^2\left(\bar{\mathbf{S}}_{i-\frac{1}{2}}^{(k)} - \lambda^1\bar{\mathbf{H}}_{i-\frac{1}{2}}^{(k)}\right)}{\lambda^2 - \lambda^1}\right]\frac{\Delta t^k}{(k+1)!} \tag{117}$$

and more generally, when considering all wave speed combinations, the resulting fluctuations read

$$\delta\mathbf{M}_{i+1/2}^{-,(k)} = \begin{cases} 0 & \text{if} \quad \lambda^1 \geq 0 \\ \delta\mathbf{M}_{i+1/2}^{-,(k),sub} & \text{if} \quad \lambda^1 \leq 0 \leq \lambda^2 \\ \widetilde{\mathbf{J}}_{i+1/2}\delta\mathbf{D}_{i+\frac{1}{2}}^{(k)}\frac{\Delta t^k}{(k+1)!} - \bar{\mathbf{S}}_{i+\frac{1}{2}}^{(k)} & \text{if} \quad \lambda^2 \leq 0 \end{cases}, \tag{118}$$

$$\delta\mathbf{M}_{i-1/2}^{+,(k)} = \begin{cases} \widetilde{\mathbf{J}}_{i+1/2}\delta\mathbf{D}_{i-\frac{1}{2}}^{(k)}\frac{\Delta t^k}{(k+1)!} - \bar{\mathbf{S}}_{i-\frac{1}{2}}^{(k)} & \text{if} \quad \lambda^1 \geq 0 \\ \delta\mathbf{M}_{i-1/2}^{+,(k),sub} & \text{if} \quad \lambda^1 \leq 0 \leq \lambda^2 \\ 0 & \text{if} \quad \lambda^2 \leq 0 \end{cases}, \tag{119}$$

6. Application to the shallow water equations

In this section, the proposed AR-ADER and HLLS-ADER methods, in their non-linear and acoustic versions, are applied to the shallow water equations

$$\mathbf{U} = \begin{pmatrix} h \\ q \end{pmatrix}, \; \mathbf{F} = \begin{pmatrix} hu \\ hu^2 + \frac{1}{2}gh^2 \end{pmatrix}, \; \mathbf{S} = \begin{pmatrix} 0 \\ S_z \end{pmatrix}, \tag{120}$$

where h is the water depth, u is the depth averaged velocity and g is the acceleration of gravity. The source term S_z involves the variations in bed geometry S_z

$$S_z = -gh\frac{dz}{dx}, \tag{121}$$

where z represents the bed elevation.

When applied to the shallow water equations, the Augmented Roe solver provides a linearized solution that can be straightforward expanded from the homogeneous case. The approximate Jacobian $\widetilde{\mathbf{J}}$ of the homogeneous part is given by [22]

$$\tilde{\mathbf{J}}_{i+1/2} = \begin{pmatrix} 0 & 1 \\ \widetilde{c}^2 - \widetilde{u}^2 & 2\widetilde{u} \end{pmatrix}_{i+1/2}, \qquad \delta\mathbf{F}_{i+1/2} = \widetilde{\mathbf{J}}_{i+1/2}\delta\mathbf{U}_{i+1/2}, \tag{122}$$

where

$$\begin{aligned} \widetilde{\lambda}^1 &= \widetilde{u} - \widetilde{c}, \qquad \widetilde{\lambda}^2 = \widetilde{u} + \widetilde{c} \\ \widetilde{\mathbf{e}}^1 &= \begin{pmatrix} 1 \\ \widetilde{u} - \widetilde{c} \end{pmatrix}, \qquad \widetilde{\mathbf{e}}^2 = \begin{pmatrix} 1 \\ \widetilde{u} + \widetilde{c} \end{pmatrix} \end{aligned} \tag{123}$$

with

$$\widetilde{c} = \sqrt{g\frac{h^{(0)}_{i_R} + h^{(0)}_{(i+1)_L}}{2}}, \qquad \widetilde{u} = \frac{u^{(0)}_{(i+1)_L}\sqrt{h^{(0)}_{(i+1)_L}} + u^{(0)}_{i_R}\sqrt{h^{(0)}_{i_R}}}{\sqrt{h^{(0)}_{(i+1)_L}} + \sqrt{h^{(0)}_{i_R}}}, \tag{124}$$

with $h^{(0)}$ and $u^{(0)}$ the spatial reconstruction of the water depth and velocity, respectively.

In order to extend the well balanced property for static equilibrium to the exactly balanced property, that ensures exact equilibrium under steady state, we use the numerical approximation proposed in [49] over the leading term of the spatial integral of the source term S_z. Such approximation is based on the principle of conservation of mechanical energy and is only applied to the leading term, since higher order terms become nil in steady state when energy is conserved. The approximation of the spatial integral of the source term inside an arbitrary interval $[x_I, x_J]$ will be referred to as

$$\int_{x_I}^{x_J} -g\, h^{(0)}\, \frac{dz}{dx} dx \approx \bar{S}^{(0)}_{z_{I,J}} \tag{125}$$

and corresponds to the leading term of (33) and (34) when $[x_I, x_J] = [x_{i_L}, x_{i_R}]$ and $[x_I, x_J] = [x_{i_R}, x_{(i+1)_L}]$ respectively. It is worth saying that hereafter, the latter will be referred to as $\bar{S}^{(0)}_{z_{i+1/2}}$. Analogously, the approximation of the spatial integral of time derivatives of the source term will be referred to as

$$\int_{x_I}^{x_J} -g\, h^{(k)}\, \frac{dz}{dx} dx \approx \bar{S}^{(k)}_{z_{I,J}}\,. \tag{126}$$

The method in [49] evaluates the discrete source term at the cell interfaces in a particular way in order to ensure the energy balance property. It proposes a combination of two alternatives: one is to compute (125) considering a smooth variation of the variables inside the interval $[x_I, x_J]$ as

$$\bar{S}^{a}_{z_{I,J}} = -g\bar{h}\delta z\,, \tag{127}$$

where

$$\bar{h} = \frac{1}{2}(h^{(0)}_J + h^{(0)}_I)\,, \qquad \delta z = z_J - z_I \tag{128}$$

and the second possibility is to define $S^{b}_{z_{I,J}}$ as

$$\bar{S}^{b}_{z_{I,J}} = -g h_j \delta z\,, \tag{129}$$

where

$$h_j = \begin{cases} h^{(0)}_I & \text{if} \quad \delta h^{(0)} > 0 \\ h^{(0)}_J & \text{if} \quad \delta h^{(0)} \leq 0 \end{cases} \tag{130}$$

with $\delta h^{(0)} = h_J^{(0)} - h_I^{(0)}$. In cases of still water with a continuous water level surface, both (127) and (129) do ensure quiescent equilibrium. In this particular case hydrostatic forces are exactly balanced. Considering the two previous options, it is possible to evaluate $\bar{S}_{z_{I,J}}^{(0)}$ as a combination of them

$$\bar{S}_{z_{I,J}}^{(0)} = (1-\mathcal{A}) S_{z_{I,J}}^{a} + \mathcal{A} S_{z_{I,J}}^{b} \,, \tag{131}$$

where $0 \leq \mathcal{A} \leq 1$. In order to satisfy both energy and momentum conservation under steady conditions, a value $\mathcal{A}_E$ is defined as

$$\mathcal{A}_E = \frac{\delta(hu^2) - \bar{h}\delta\left(\frac{u^2}{2}\right)}{S_{z_{I,J}}^{b} - S_{z_{I,J}}^{a}} \,, \tag{132}$$

according to [49]. Coefficient $\mathcal{A}_E$ in (132) can be used in (131) to ensure the conservation of energy for smooth solutions. On the other hand, when considering transcritical jumps, energy must be dissipated, hence the value of weight coefficient $\mathcal{A}$ in (131) is set to 1. Considering these situations, the complete algorithm for the calculation of $\mathcal{A}$ reads [49]

$$\mathcal{A} = \begin{cases} \mathcal{A}_E & \text{if } u_J^{(0)} u_I^{(0)} > 0 \text{ and } |Fr_J| > 1 \text{ and } |Fr_I| > 1 \\ \mathcal{A}_E & \text{if } u_J^{(0)} u_I^{(0)} > 0 \text{ and } |Fr_J| < 1 \text{ and } |Fr_I| < 1 \\ 1 & \text{otherwise} \end{cases} \tag{133}$$

where Fr_I and Fr_J are the Froude numbers at positions I and J respectively.

By using this technique, quiescent equilibrium is guaranteed in cases of still water, while in steady cases with smooth solutions exact conservation of energy is preserved. In presence of hydraulic jumps, energy is dissipated at the correct rate. This numerical technique allows both the AR-ADER scheme and HLLS-ADER scheme to evaluate the source strengths, $\beta^{(0),m}$, and matrix $\bar{\mathbf{H}}_{i+\frac{1}{2}}^{(0)}$ respectively, ensuring an exact balance between fluxes and source terms. Moreover, it can be used to approximate the integral of the source term inside the cells.

Under steady conditions, the water discharge is constant along the spatial coordinate and moreover, if variations are smooth, the mechanical energy is also constant. In order to preserve the energy balanced property, the spatial reconstruction must be carried out for the specific mechanical energy and the unitary discharge

$$E = \frac{u^2}{2g} + h + z\,, \qquad q = hu\,. \tag{134}$$

Then, variables h and u are computed departing from spatial reconstructions of E and q.

Time derivatives of the fluxes, conserved variables and sources in equations (19)-(23) are computed by means of spatial derivatives of the conserved variables using the Cauchy-Kowalewski theorem. When carrying out this procedure, time derivatives should be expressed as a sum of terms where spatial derivatives of E and q are common factors. In this way, functions $\mathbf{R}^{(k)}$, $\mathbf{D}^{(k)}$ and $\mathbf{Q}^{(k)}$ become nil as there is no spatial variation of energy or discharge, ensuring the discrete equilibrium.

With this information, it is possible to compute the contribution of the source term across the cell edge in (34) by means of (131) for the leading term

$$\bar{S}^{\,(0)}_{2_{i+1/2}} = \bar{S}^{\,(0)}_{z_{i+1/2}} = (1-\mathcal{A})S^{a}_{z_{i+1/2}} + \mathcal{A}S^{b}_{z_{i+1/2}}\,, \tag{135}$$

and using the following discretization for the high order terms

$$\bar{S}^{\,(k)}_{2_{i+1/2}} = \frac{1}{\Delta t}\int_0^{\Delta t}\int_{x^-_{i+1/2}}^{x^+_{i+1/2}} -g\,h^{(k)}\,\frac{dz}{dx}dx \approx -g\left(\frac{h^{(k)}_{(i+1)_L} + h^{(k)}_{i_R}}{2}\right)\delta z \tag{136}$$

with $\delta z = z_{(i+1)_L} - z_{i_R}$.

6.1. Energy balanced integration of the source term inside the cell

When constructing first order augmented schemes, the conservation of energy was only imposed in the discretization of the source term at cell interfaces [49] since variations of the variables along the cell length were nil. When moving to high order schemes of the ADER type, where spatial variations of the variables along the cell do exist, the conservation of energy must also be taken into account in the calculation of the integral of the source term inside the cell. Only when the energy balanced approach is used, an exact equilibrium between fluxes and source term is obtained. It can be shown that only when the source term is integrated exactly, it is possible to construct an energy balanced scheme; on the other hand, if using traditional quadrature rules for its approximation, the numerical scheme will converge to

the exact solution under steady conditions when the grid is refined, instead of directly providing the exact solution. In order to show this, let us consider the equations for the conservation of momentum and energy under steady state conditions, that is $\partial_x E = \partial_x hu = 0$,

$$\frac{\partial}{\partial x}\left(hu^2 + \frac{1}{2}gh^2\right) = -gh\frac{dz}{dx}\,, \tag{137}$$

$$\frac{\partial}{\partial x}\left(\frac{1}{2}u^2 + g(h+z)\right) = 0\,, \tag{138}$$

considering smooth variations of the variables. Expanding equation (137), it yields

$$hu\frac{\partial u}{\partial x} + u\frac{\partial (hu)}{\partial x} + gh\frac{\partial h}{\partial x} = -gh\frac{dz}{dx}\,, \tag{139}$$

and considering that the second term is nil under steady conditions, it can be simplified to

$$hu\frac{\partial u}{\partial x} + gh\frac{\partial h}{\partial x} = -gh\frac{dz}{dx}\,, \tag{140}$$

On the other hand, multiplying equation (138) by h and rearranging the terms, it yields

$$gh\frac{\partial h}{\partial x} = -hu\frac{\partial u}{\partial x} - gh\frac{dz}{dx}\,, \tag{141}$$

Substitution of (141) in (140) proves that the equality is fulfilled. With this result, it is evidenced that under steady conditions, energy is conserved and variations of momentum are due to the thrust exerted by changes on the bed elevation. More importantly, it also proves that in the discrete level, an exact integration of the source term leads to the exact equilibrium.

Let us consider again equations (137) and (138), but now in their discrete form

$$\delta\left(hu^2 + \frac{1}{2}gh^2\right) = -g\bar{h}\delta z + \breve{s}\,, \tag{142}$$

$$\delta\left(\frac{1}{2}u^2 + g(h+z)\right) = 0\,, \tag{143}$$

and notice that the source term has been approached by the trapezoidal rule as

$$\int -gh\frac{dz}{dx}dx = -g\bar{h}\delta z + \breve{s}\,, \tag{144}$$

where $\breve{s}$ is the residual of the approximation and operator

$$\bar{(\cdot)} = \frac{(\cdot)_I + (\cdot)_J}{2} \tag{145}$$

is a conventional average operator. When expanding (142), it can be written as

$$\overline{hu}\delta u + \bar{u}\delta(hu) + g\bar{h}\delta h = -g\bar{h}\delta z + \breve{s}\,, \tag{146}$$

where $\bar{u}\delta(hu) = 0$, yielding

$$\overline{hu}\delta u + g\bar{h}\delta h = -g\bar{h}\delta z + \breve{s}\,. \tag{147}$$

Multiplying (143) by $\bar{h}$, we have

$$g\bar{h}\delta h = -\bar{h}\bar{u}\delta u - g\bar{h}\delta z\,, \tag{148}$$

that can be inserted in (147), leading to

$$(\overline{hu} - \bar{h}\bar{u})\delta u = \breve{s}\,. \tag{149}$$

The result obtained in (149) is of paramount importance, as it represents the correction of the source term to be made in order to exactly balance the difference of fluxes. It is evidence that the reason why the correction must be made is that $\widetilde{hu} \neq \widetilde{h}\widetilde{u}$. It is worth showing that $\breve{s}$ can also be written as

$$\breve{s} = \delta(hu^2) - \bar{h}\delta\left(\frac{1}{2}u^2\right) = \mathcal{A}(S_z^b - S_z^a)\,, \tag{150}$$

using the definition of $\mathcal{A}$ in [49]. In this way, the correction in (149) or (150) can be given a physical meaning, that is the difference between the differential discretization, S_z^a, and the integral discretization, S_z^b. In [45], they showed that $\breve{s}$ can be rewritten as a third order difference

$$\breve{s} = \frac{1}{4}\delta h\,(\delta u)^2\,. \tag{151}$$

Taking all these things into account, the energy balanced approach in (131) inside an arbitrary interval $[x_I, x_J]$ can be regarded as a trapezoidal integration rule plus the correcting term in (149)-(151)

$$\bar{S}^{(0)}_{z_{I,J}} = S^{a}_{z_{I,J}} + \breve{s} \tag{152}$$

where $S^{a}_{z_{I,J}} = -g\bar{h}\delta z$ and $\breve{s} = \mathcal{A}(S^{b}_{z_{I,J}} - S^{a}_{z_{I,J}})$. As outlined before, the correcting term is a third-order difference and therefore (152) is second-order accurate as a quadrature for the source term [45].

This option is suitable for third order ADER schemes, but it may prevent higher order schemes from reaching the theoretical order of accuracy. In [1], the approximation in equation (153) was used, leading to an energy balanced numerical scheme that appeared to be suboptimal for the water depth in certain cases when the order of accuracy was set to 5. When using this strategy, the centered contributions of the leading term of the source in (34) reads

$$\bar{S}_{2}{}^{(0)}_{i_R,i_L} = \bar{S}{}^{(0)}_{z i_R,i_L} = (1-\mathcal{A}) S^{a}_{z i_R,i_L} + \mathcal{A} S^{b}_{z i_R,i_L}\,, \tag{153}$$

with (153) calculated inside the interval $[x_I, x_J] = [x_{i_L}, x_{i_R}]$, using definitions in (127)-(131). As outlined before, the integral of the high order terms of the source need not be energy balanced. Using the trapezoidal rule, it can be approximated by

$$\bar{S}_{2}{}^{(k)}_{i_R,i_L} = -g\left(\frac{h^{(k)}_{i_R} + h^{(k)}_{i_L}}{2}\right)\delta z \frac{\Delta t^k}{(k+1)!}\,, \tag{154}$$

with $\delta z = z_{i_R} - z_{i_L}$.

It is evidenced that difficulties may arise when constructing high order energy balanced numerical schemes, as it may become a hard task to preserve the discrete energy balance property while ensuring the theoretical order of accuracy. To address this issue, in [45] a fifth order energy balanced scheme was constructed by approximating the mentioned integral by a fourth order extrapolation of a second order energy balanced discretization of the source term.

In the present work, the approach in [45] is followed and the second order approximation of the integral of the source term provided by (131) is extended to higher order by extrapolation. The resulting approximation of the integral will now be of arbitrary order while still ensuring the conservation of energy,

however, the computational cost will be higher since a recursive procedure is required to carry out the extrapolation.

The keystone of this method is to use Richardson's extrapolation for the acceleration of convergence of the integral of the source term by means of the so-called Romberg integration, which relates two numerical quadratures with different step sizes, hereafter denoted by l, and combines them to generate a higher order approximation. For the trapezoidal rule, the error of the quadrature can be expressed in power series only involving even powers of l. This idea can be extended to the corrected quadrature formula for the integral of the source term in (131), that according to [45] reads

$$\int_{x_{i_L}}^{x_{i_R}} -gh\frac{dz}{dx}dx = \bar{S}^{(0)}_{z_{i_R,i_L}} + a_1 l^2 + a_2 l^4 + a_3 l^6 + \dots . \tag{155}$$

Making use of Richardson improvement, combination of equation (155) for l and $2l$ allows to eliminate a_1, and so on for the other constants. In this way, as the lower order terms of the error become nil, a higher order quadrature is obtained. The general algorithm for Richardson's extrapolation can be found in [55].

6.2. Asymptotically energy balanced integration of the source term inside the cell

The use of traditional quadrature rules for the integral of the source term inside the cell is also studied in the present work. When using such approximation of the integrals, the numerical scheme is unable to keep a constant level of energy and therefore it cannot be considered as an energy balanced scheme. However, if RPs have been solved considering the conservation of energy, it can be proven that the use of traditional quadrature rules allows the scheme to converge to the exact solution when the grid is refined.

In this work, ADER schemes using traditional quadrature rules for the centered integration of the source term will be referred to as asymptotically energy balanced schemes. They are given such a name since they do converge to the energy balanced solution when the grid is refined while retaining the prescribed order of accuracy. To construct an asymptotically energy balanced scheme, the integral of the source term inside the cell must be approximated by means of a suitable quadrature formula that ensures the prescribed order of accuracy.

In this work, we use Gaussian quadrature, which requires to reconstruct information at k points, the Gaussian points, in order to calculate a $2k-1$-th order integral. Integrals in (33) will read

$$\bar{S}_{2i_R,i_L}^{(0)} = \bar{S}_{zi_R,i_L}^{(0)}\,, \tag{156}$$

$$\bar{S}_{2i_R,i_L}^{(k)} = \bar{S}_{zi_R,i_L}^{(k)} \frac{\Delta t^k}{(k+1)!}\,, \tag{157}$$

with

$$\bar{S}_{zi_R,i_L}^{(0)} = \frac{\Delta x}{2} \sum_{j=1}^{k} w_j \left(-g\, h^{(0)} \frac{dz}{dx} \right)_{x=x_j^c}\,, \tag{158}$$

$$\bar{S}_{zi_R,i_L}^{(k)} = \frac{\Delta x}{2} \sum_{j=1}^{k} w_j \left(-g\, h^{(k)} \frac{dz}{dx} \right)_{x=x_j^c}\,, \tag{159}$$

where $x_j^c = x_{i-1/2} + (x_j^g + 1)\Delta x/2$ are the quadrature points inside the cell, x_j^g are the Gaussian quadrature points inside the interval of reference $[-1, 1]$ and w_j the Gaussian weights at those points. It is worth mentioning that the approximation of the integral by Gaussian quadrature requires a lower computational effort than using the proposed energy balanced high order extrapolation.

6.3. Numerical solution of steady cases

The energy balance approach in [49] ensures a constant value of mechanical energy, with the property of providing the exact solution at every computational cell under steady conditions with independence of the grid refinement. Such property allows to construct a so-called energy balanced numerical scheme. In this work, approach in [49] has been used for the discretization of the leading term of the source as provided in equation (131), leading to an arbitrary order energy balanced scheme.

In [1], numerical results provided by the AR-ADER scheme for steady flow over a hump were presented for three different flow regimes. The numerical scheme proved to provide the exact solution with independence of the cell size.

When repeating the test case of steady flow over a hump in [1] for the HLLS-ADER scheme and for the acoustic approaches, the same behavior is

observed. All schemes converge to the exact solution with independence of the grid refinement. In this section, the test case of subcritical flow over a hump is used to demonstrate that both the AR-ADER scheme and the HLLS-ADER schemes are energy balanced and also to evidence that an specific energy-preserving quadrature rule must be used to compute the integral of the source inside the cell. To this end, numerical results obtained when using energy balanced Romberg approach and a traditional Gaussian quadrature rule are be shown. It is worth recalling that the numerical scheme is referred to as asymptotically energy balanced when using the Gaussian quadrature rule for the integral of the source term.

The test case is set up as follows. The bed elevation is given by the following function

$$z(x) = \begin{cases} 0 & \text{if} \quad x < 8 \\ 0.2 - 0.05\,(x-10)^2 & \text{if} \quad 8 \leq x \leq 12 \\ 0 & \text{if} \quad x > 12 \end{cases} \tag{160}$$

inside the domain $[0, 25]$ and the boundary conditions are set to $q = 4.42$ m^2/s at the inlet and $h = 2$ m at the outlet. CFL is set to 0.3 and the acceleration of gravity to 9.8 m/s^2. Figure 6 shows the numerical results for energy (left) and discharge (right) provided by the AR-ADER and HLLS-ADER schemes when using energy balanced Romberg approach and a Gaussian quadrature rule for the integration source term. Plots on the top correspond show numerical results computed using 100 cells whereas those in the bottom are computed using 200 cells.

It is observed that only when using an energy balanced discretization of the source term at cell interfaces and an energy balanced integration of the source term inside the cell, the exact solution is obtained. This is the case of the AR-ADER schemes and HLLS-ADER schemes in combination with the energy balanced Romberg integration of the source term. In Figure 6, it can be observed that both schemes provide a constant energy value of $E = 2+4.42^2/8g$ m and a constant discharge of $q = 4.42$ m^2/s. On the other hand, when considering other quadrature rules such as the Gaussian quadrature rule used in this case for the AR-ADER and HLLS-ADER schemes, energy conservation is not ensured and the numerical scheme is unable to converge to the exact solution, as observed in Figure 6.

It is worth recalling that the energy balance discretization of the source term in (135) has been used for all cases when solving the RPs. Considering

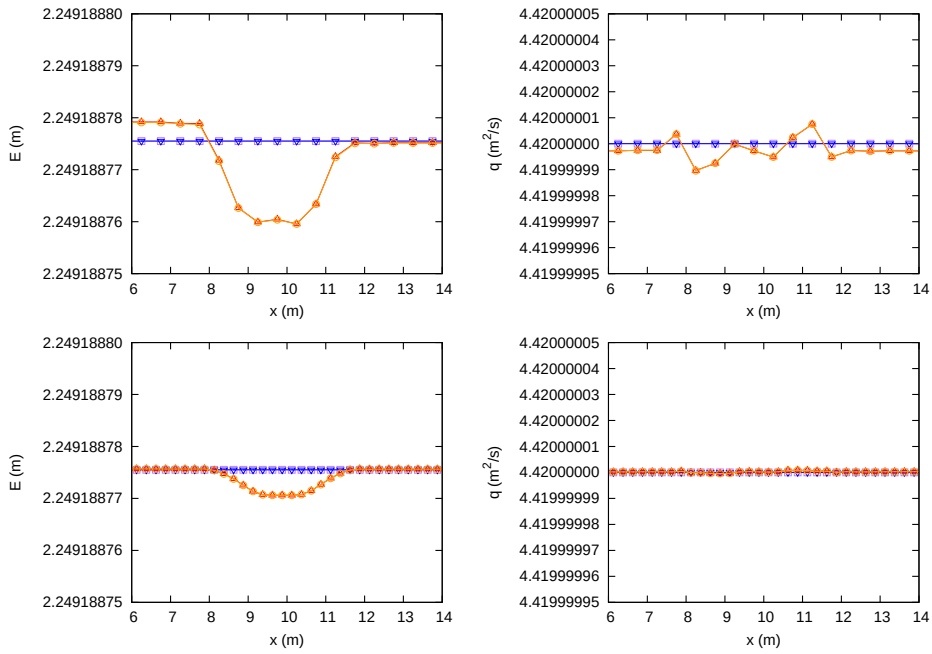

Figure 6: Section 6.3. Exact solution (–) and numerical solution provided by a 3rd order energy balanced AR-ADER scheme (–□–), 3rd order energy balanced HLLS-ADER scheme (–▽–), 3rd order asymptotically energy balanced AR-ADER scheme (– ○ –) and 3rd order asymptotically energy balanced HLLS-ADER scheme (–△–),

the previous results and those from [49], it is evidenced that the numerical scheme converges to the exact solution only when the energy balanced approach in (135) is considered in the resolution of the RPs and, moreover, it provides the exact solution for steady states when an energy balanced quadrature for the integral of the source term inside the cell is used. The numerical scheme under these assumptions is exact energy balanced. Otherwise, the numerical scheme does not provide the exact solution directly but converges to it, as the numerical scheme under these assumptions would be asymptotically energy balanced.

6.4. Numerical performance in RP

Comparison between exact solutions of different Riemann problems for system (120) and numerical solutions for the same problems provided by the AR-ADER, ARL-ADER, HLLS-ADER and HLLSL-ADER methods are next presented. 4 Different RPs are proposed and their numerical solution for water surface elevation, $h+z$, and unitary flow, q, will be presented separately for each numerical scheme. The examples involve different combinations of wave patterns in presence of bed discontinuities and are summarized in Table 1. It is worth saying that cases 2 and 3 are included in a list of RPs defined by LeFloch and Duc-Thanh [35]. The domain is defined by $[-0.5, 0.5]$ m, the bottom step is positioned at $x = 0$, has a variable height and the acceleration of gravity is set to g=9.8 m/s^2. The domain is divided in 500 cells and 1000 cells to see if the schemes converge when the grid is refined. Numerical solutions are plotted at time $t = 0.01$ s.

RP	h_L	h_R	u_L	u_R	z_L	z_R
1	4.0	0.69196567	0.0	0.0	0.0	1.5
2	0.3	0.39680194	2.0	2.2	1.0	1.0
3	1.0	1.2	3.0	0.1	1.1	1.0
4	1.0	2.0	2.0	4.0	1.1	1.0

Table 1: Section 6.4. Summary of test cases.

RP 1 is a dam-break type problem whose initial condition consists of two columns of water of different height and zero velocity, with a discontinuity in bed elevation. The solution contains a left-moving rarefaction wave, a stationary discontinuity at the step and a right-moving shock wave. Numerical

solutions are compared with the exact solution in Figures 7, 8, 9, 10. The four numerical schemes prove to converge to the exact solution in the whole computational domain when the grid is refined and are able to accurately capture the stationary discontinuity generated by the source term at the origin. When comparing the numerical solutions provided by the four schemes, it is possible to notice that the HLLS-ADER scheme provide a less diffusive numerical solution than the others. There are not noticeable differences between the AR-ADER, the ARL-ADER and the HLLSL-ADER schemes.

Supercritical motion from left to right is considered in RP 2. Numerical solutions are compared with the exact solution in Figures 11, 12, 13, 14. The four numerical schemes prove to converge to the exact solution when the grid is refined. It is observed that the presence of the discontinuity in bed elevation at $x = 0$ does not introduce any disturbance in the wave patterns on the right side. When seeking differences among the numerical solutions provided by the different schemes, it is possible to observe that the numerical solution provided by the HLLS-ADER scheme is slightly less diffusive than those solutions provided by the other methods, among which no relevant differences can be found.

RP 3 is a resonance problem that admits only one solution given by a sequence of shocks. Numerical solutions are compared with the exact solution in Figures 15, 16, 17, 18. It can be observed that the four numerical schemes prove to converge to the exact solution when the grid is refined. Here, numerical results evidence again that the HLLS-ADER scheme provides a more accurate solution around discontinuities.

As a general observation on the previous test cases, we can say that all the numerical schemes provide accurate results for the water level surface and unitary discharge at the bed discontinuity and convergence is ensured with mesh refinement or when numerical order is increased.

RP 4 also is a resonant problem that admits only one solution. The solution begins with a rarefaction, followed by a stationary contact, continued by a shock wave and finally ends in a rarefaction. Numerical solutions are compared with the exact solution in Figures 19, 20, 21, 22. When using ARoe type schemes, namely the AR-ADER and the ARL-ADER schemes, the numerical solution converges to the exact solution. On the other hand, when using HLLS-type schemes for RP 4, namely the HLLS-ADER and HLLSL-ADER schemes, such methods are unable to converge to the exact solution, as shown in Figures 21 and 22. This can be caused due to an improper choice of the wave celerities.

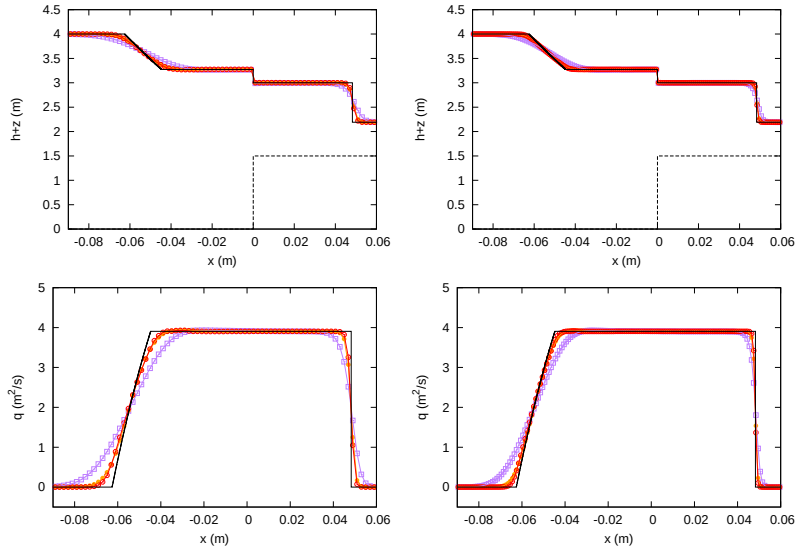

Figure 7: Section 6.4. RP 1. Exact solution (—) and numerical solutions using the 1st (–□–), 3rd (– ● –) and 5th (– ○ –) order AR-ADER method using (left) 500 and (right) 1000 cells.

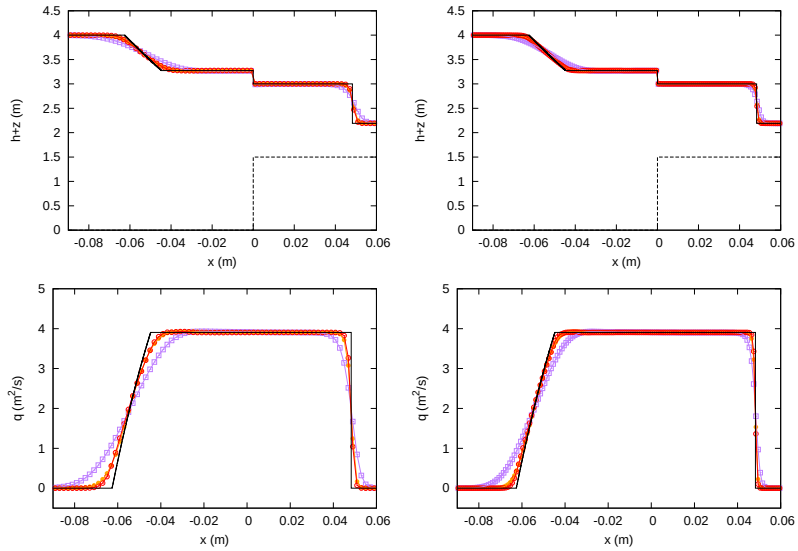

Figure 8: Section 6.4. RP 1. Exact solution (—) and numerical solutions using the 1st (–□–), 3rd (– ● –) and 5th (– ○ –) order ARL-ADER method using (left) 500 and (right) 1000 cells.

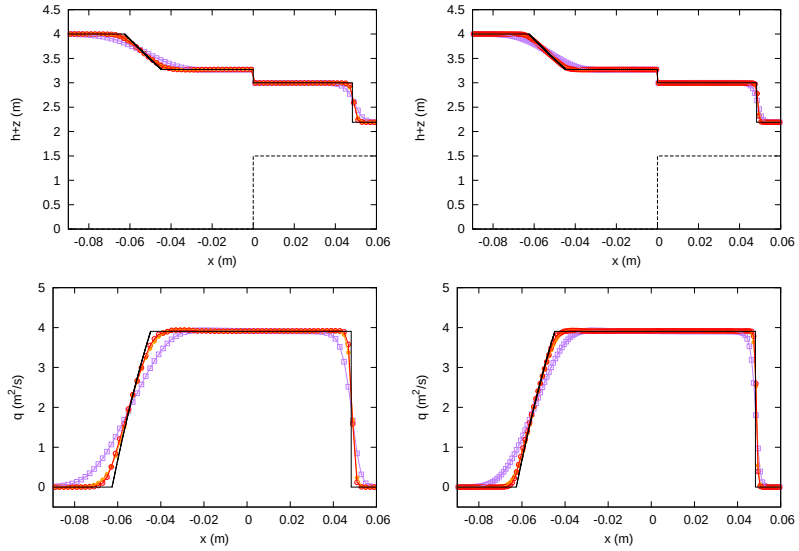

Figure 9: Section 6.4. RP 1. Exact solution (—) and numerical solutions using the 1st (–□–), 3rd (–●–) and 5th (–○–) order HLLS-ADER method using (left) 500 and (right) 1000 cells.

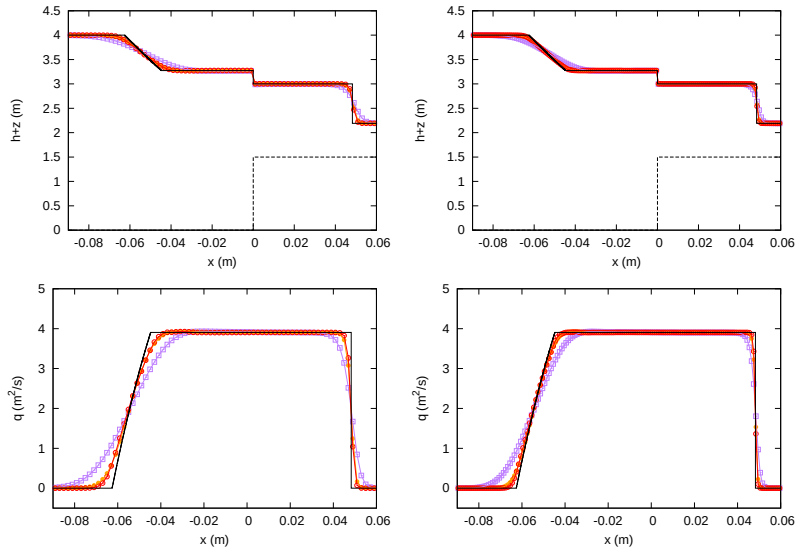

Figure 10: Section 6.4. RP 1. Exact solution (—) and numerical solutions using the 1st (–□–), 3rd (–●–) and 5th (–○–) order HLLSL-ADER method using (left) 500 and (right) 1000 cells.

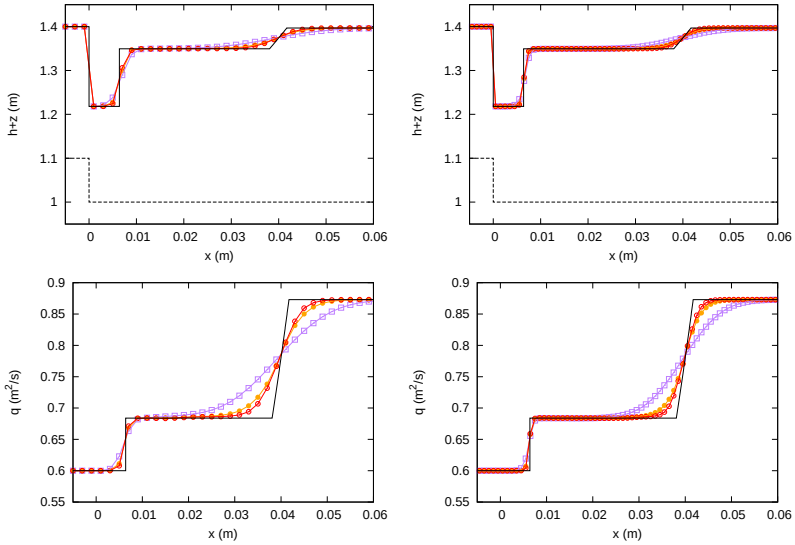

Figure 11: Section 6.4. RP 2. Exact solution (—) and numerical solutions using the 1st (–□–), 3rd (– ● –) and 5th (– ○ –) order AR-ADER method using (left) 500 and (right) 1000 cells.

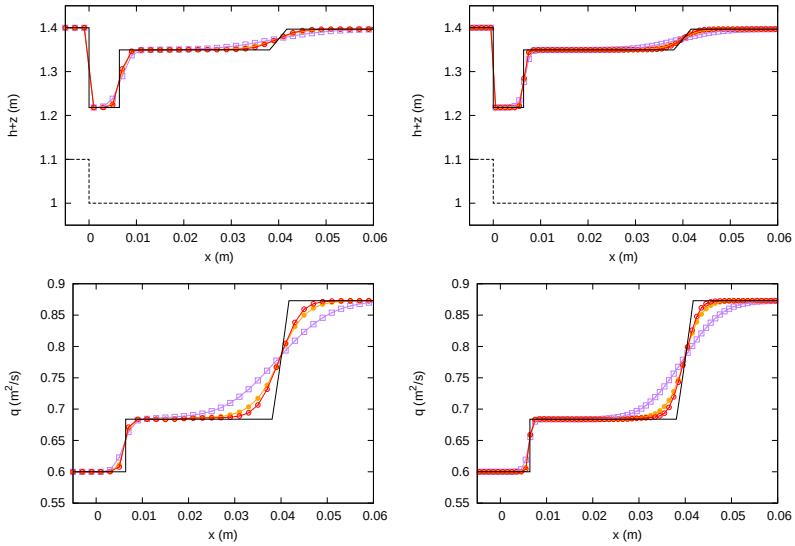

Figure 12: Section 6.4. RP 2. Exact solution (—) and numerical solutions using the 1st (–□–), 3rd (– ● –) and 5th (– ○ –) order ARL-ADER method using (left) 500 and (right) 1000 cells.

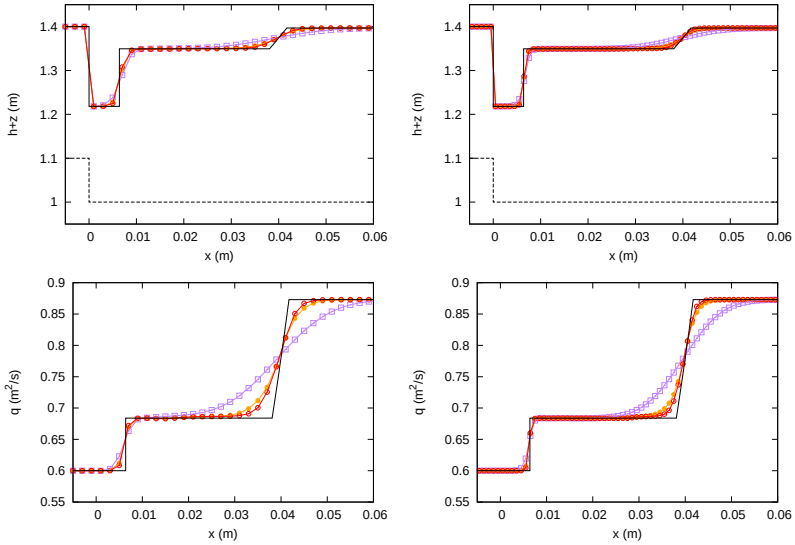

Figure 13: Section 6.4. RP 2. Exact solution (—) and numerical solutions using the 1st (–□–), 3rd (– ● –) and 5th (– ○ –) order HLLS-ADER method using (left) 500 and (right) 1000 cells.

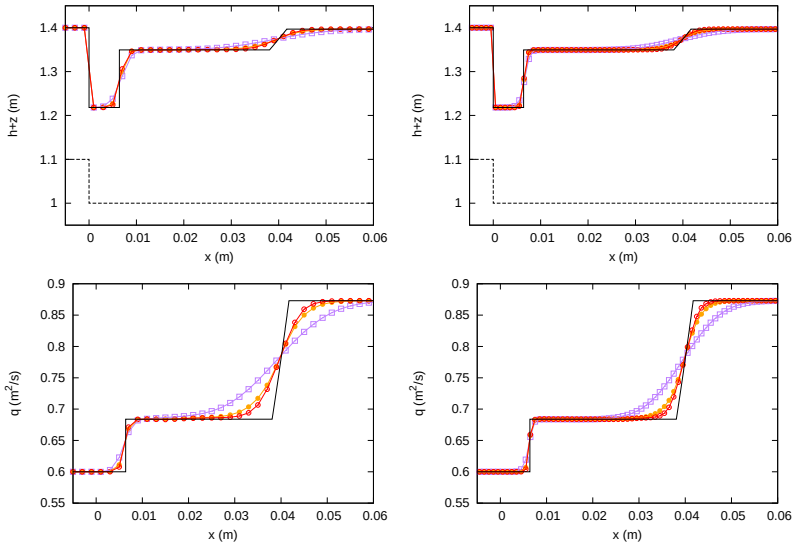

Figure 14: Section 6.4. RP 2. Exact solution (—) and numerical solutions using the 1st (–□–), 3rd (– ● –) and 5th (– ○ –) order HLLSL-ADER method using (left) 500 and (right) 1000 cells.

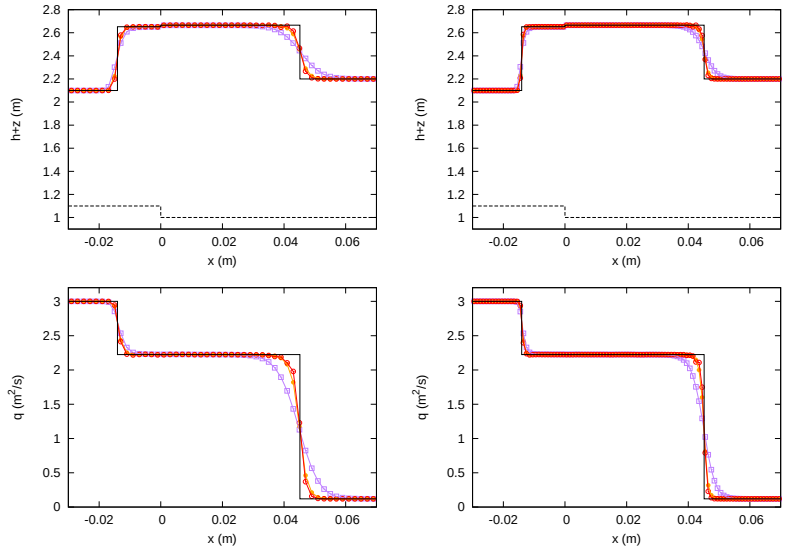

Figure 15: Section 6.4. RP 3. Exact solution (—) and numerical solutions using the 1st (–□–), 3rd (– ● –) and 5th (– ○ –) order AR-ADER method using (left) 500 and (right) 1000 cells.

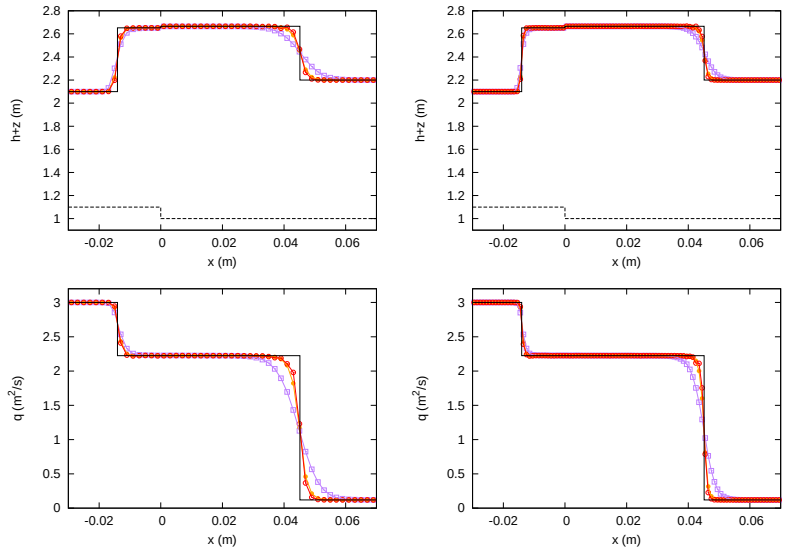

Figure 16: Section 6.4. RP 3. Exact solution (—) and numerical solutions using the 1st (–□–), 3rd (– ● –) and 5th (– ○ –) order ARL-ADER method using (left) 500 and (right) 1000 cells.

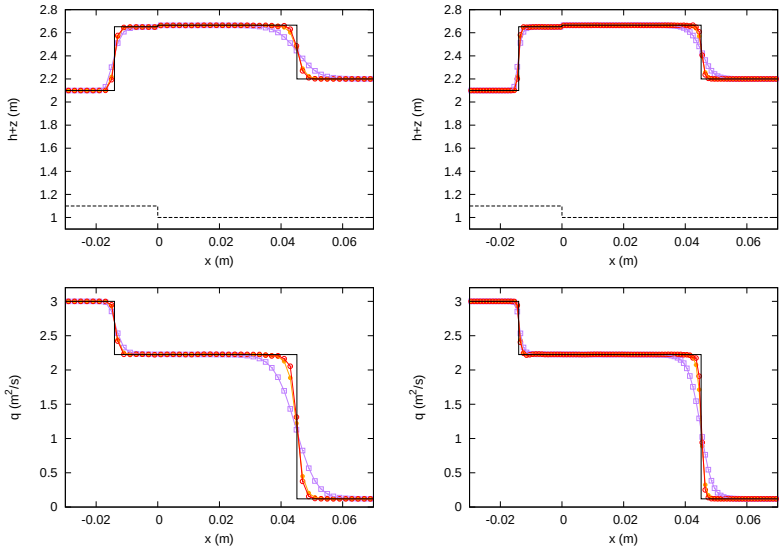

Figure 17: Section 6.4. RP 3. Exact solution (—) and numerical solutions using the 1st (–□–), 3rd (– ● –) and 5th (– ○ –) order HLLS-ADER method using (left) 500 and (right) 1000 cells.

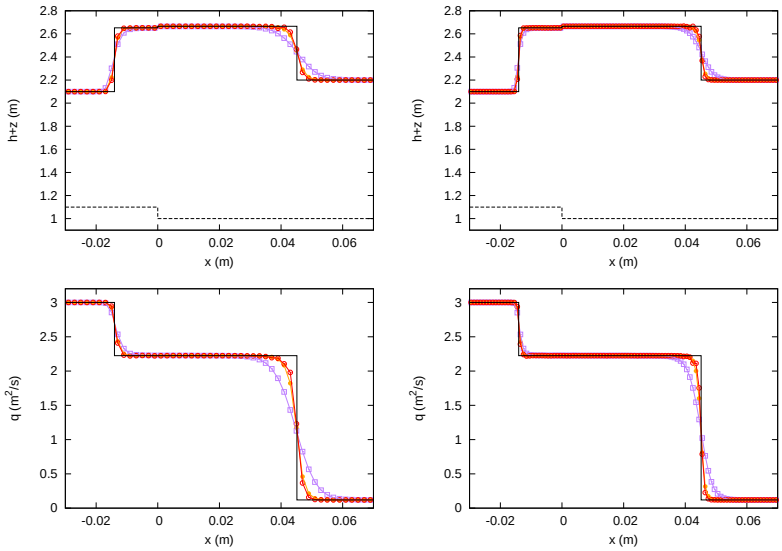

Figure 18: Section 6.4. RP 3. Exact solution (—) and numerical solutions using the 1st (–□–), 3rd (– ● –) and 5th (– ○ –) order HLLSL-ADER method using (left) 500 and (right) 1000 cells.

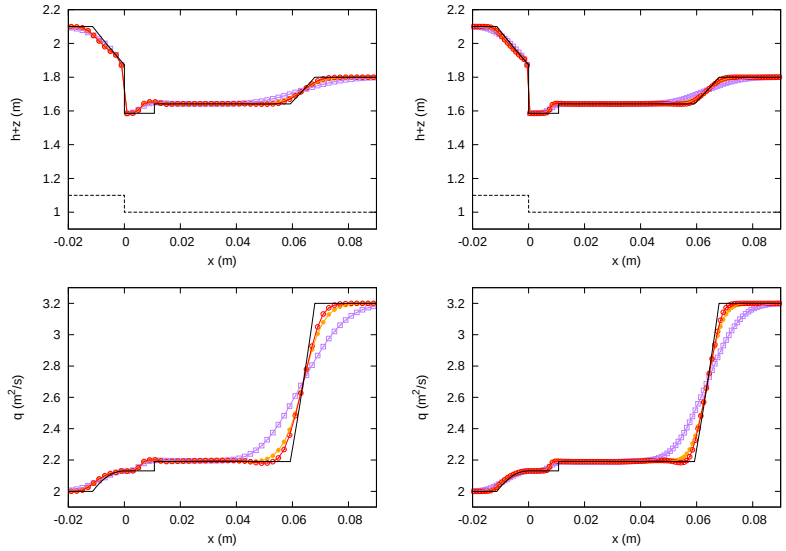

Figure 19: Section 6.4. RP 4. Exact solution (—) and numerical solutions using the 1st (–□–), 3rd (– ● –) and 5th (– ○ –) order AR-ADER method using (left) 500 and (right) 1000 cells.

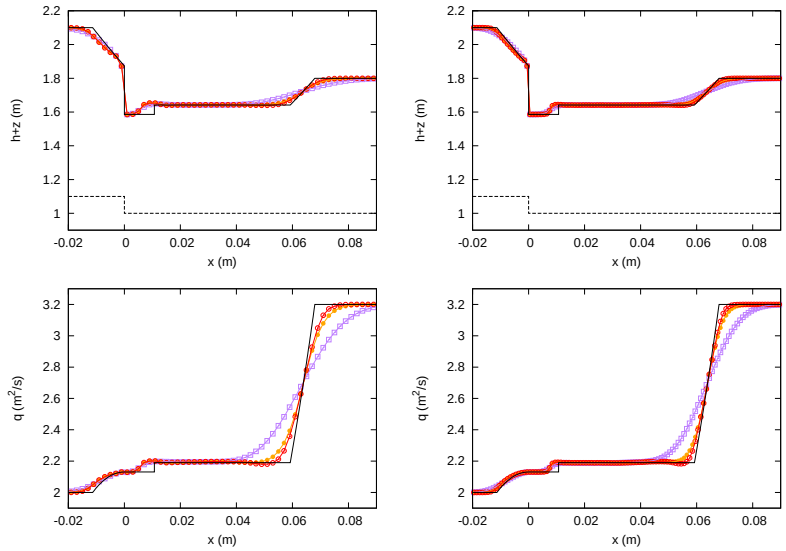

Figure 20: Section 6.4. RP 4. Exact solution (—) and numerical solutions using the 1st (–□–), 3rd (– ● –) and 5th (– ○ –) order ARL-ADER method using (left) 500 and (right) 1000 cells.

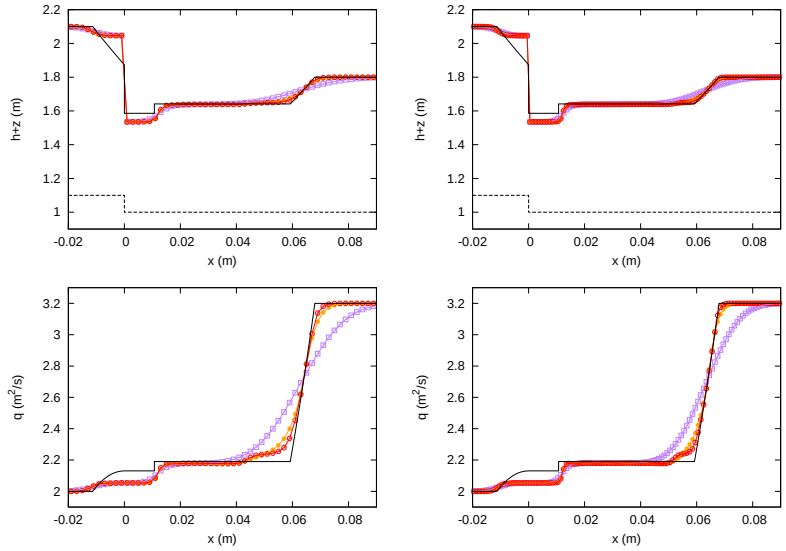

Figure 21: Section 6.4. RP 4. Exact solution (—) and numerical solutions using the 1st (–□–), 3rd (– ● –) and 5th (– ○ –) order HLLS-ADER method using (left) 500 and (right) 1000 cells.

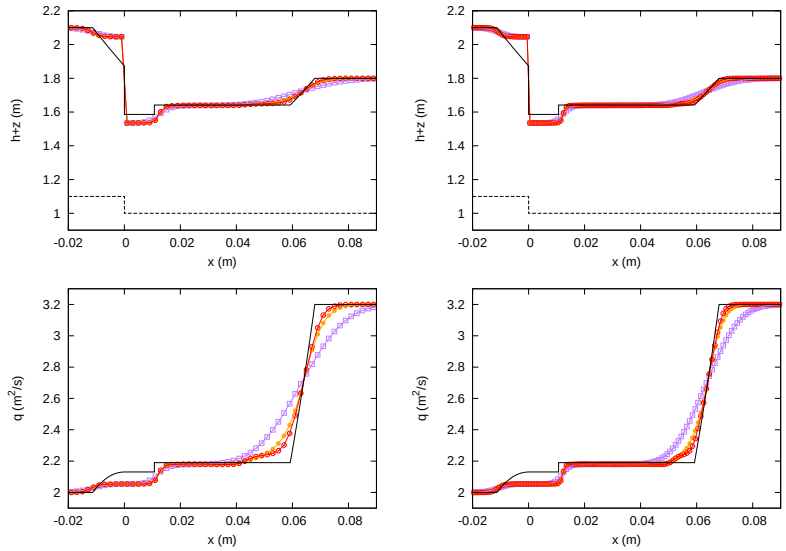

Figure 22: Section 6.4. RP 4. Exact solution (—) and numerical solutions using the 1st (–□–), 3rd (– ● –) and 5th (– ○ –) order HLLSL-ADER method using (left) 500 and (right) 1000 cells.

6.5. Convergence rate test

The following test case corresponds to the computation of the evolution of a smooth initial condition over a smooth bed elevation, given by

$$z(x) = \begin{cases} 0 & \text{if} \quad x < 2 \\ 0.01 \sin(\pi x)^4 & \text{if} \quad 2 \leq x \leq 3 \\ 0 & \text{if} \quad x > 3 \end{cases} \tag{161}$$

$$h(x,0) = 0.5 + z(x)\,, \qquad q(x,0) = 0 \tag{162}$$

inside the spatial domain $\Omega = [0,5]$ with $x \in \Omega$. The initial condition for the water depth in (162), setting the unitary discharge to zero at the initial time, leads to two symmetric waves that move in opposite directions, as shown in Figures 23a and 23b. Numerical results are computed using the first order ARoe and HLLS schemes, as well as their higher order ADER versions presented in this work, setting CFL to 0.3. Such solutions are compared with a reference solution, computed with a 5-th order AR-ADER scheme using 8000 cells. Numerical solutions for water surface elevation and unitary discharge provided by all the numerical schemes as well as the reference solution for such quantities are plotted at time $t = 0.2$ s in Figures 23a and 23b respectively.

Numerical errors provided by the first order Godunov scheme at $t = 0.2$ s are measured using L_1 and L_2 error norms and presented in Table 2. It is worth mentioning that both the ARoe and the HLLS schemes provide the same solution in this particular case when using their first order version. In Tables 3 - 6 numerical errors provided by the 3-rd and 5-th order AR-ADER, ARL-ADER, HLLS-ADER and HLLSL-ADER asymptotically energy balanced schemes, in which Gaussian quadrature is used, are presented. On the other hand, from Table 7 to Table 10, numerical errors for the exact energy balanced version of such schemes are presented.

Convergence rate tests have been carried out setting CFL=0.3 for the AR-ADER and HLLS-ADER schemes and CFL=0.05 for their linearized version, the ARL-ADER and HLLSL-ADER schemes. It is worth pointing out that, for all numerical schemes, the time step is dynamically computed using wave celerities from Roe's approximate Jacobian in (123) and corrected by the CFL number as follows

$$\Delta t = \text{CFL} \cdot \frac{\Delta x}{\max\left\{\left|\tilde{\lambda}_j^m\right|\right\}} \tag{163}$$

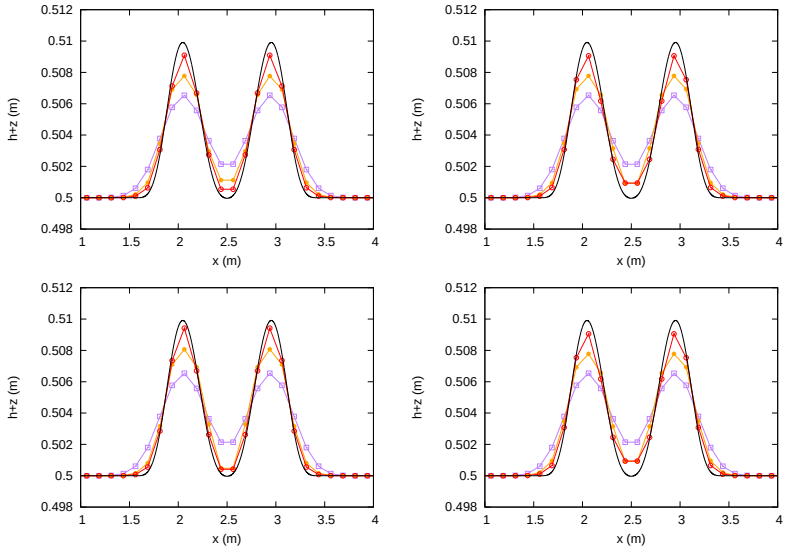

(a) Refined solution and numerical solutions for the water surface elevation $h + z$.

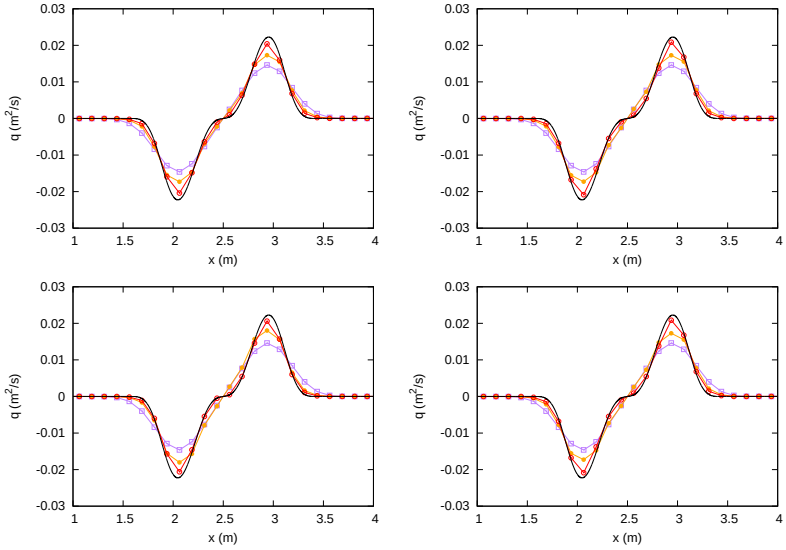

(b) Refined solution and numerical solutions for the discharge q.

Figure 23: Section 6.5. Refined solution (—) and numerical solutions for the water surface elevation $h + z$ and discharge q using the 1st (—□—), 3rd (— ● —) and 5th (— ○ —) order AR-ADER scheme (upper left), ARL-ADER scheme (upper right), HLLS-ADER scheme (lower left) and HLLSL-ADER scheme (lower right), using 40 cells.

with $j = \frac{1}{2}, ..., N + \frac{1}{2}$ and $m = 1, 2$, in order to ensure stability.

Numerical results in Tables 2 - 10 evidence that all the numerical schemes converge to the reference solution at the prescribed rate. However, it is observed a slightly faster convergence rate for the asymptotically energy balanced schemes since the approximation of the integral of the source term inside the cell is optimal in which refers to the order of convergence.

It has been observed that those numerical schemes using the LFS solver, namely the ARL-ADER and HLLSL-ADER schemes, are not able to ensure the prescribed accuracy for high CFL numbers as those schemes using the FS solver do. To study this particular behavior, we have repeated the convergence rate tests using different CFL numbers for the 3rd and 5th order HLLS-ADER and HLLSL-ADER schemes. Numerical results are presented in Figure 24 for CFL= 0.6, CFL= 0.3, CFL= 0.15 and CFL= 0.08. It is observed that the 3rd order version of the HLLS-ADER and HLLSL-ADER scheme do converge at the expected rate. However, when considering the 5th order version of such schemes, the HLLS-ADER scheme does converge at the prescribed rate but the HLLSL-ADER scheme appears to be suboptimal. Only when using the lowest CFL number the HLLSL-ADER scheme converges to the exact solution at the expected rate. This behavior is due to the linearization that has been carried out to construct the HLLSL-ADER scheme by means of the LFS Derivative Riemann solver. Similar results have been reported for the AR-ADER and ARL-ADER schemes.

Therefore, the choice of such a small CFL number when using the linearized LFS solver is related to the recovery of the optimal accuracy of the numerical scheme rather than to any issue related to stability. When setting the CFL number to 0.3 or even higher, LFS-based schemes, namely the ARL-ADER and HLLSL-ADER, are stable and still converge to the reference solution, however, their convergence rate is suboptimal as Figure 24 shows.

CPU times for the present test case when using the 3rd and 5th order energy balanced HLLSL-ADER, HLLS-ADER, ARL-ADER and AR-ADER schemes are presented in Table 11. The simulation time is set to $t = 3$ s and the CFL number to 0.3. Results are presented for two different grids composed of 80 and 160 cells respectively. Speed-ups of the linearized schemes, namely HLLSL-ADER and ARL-ADER, with respect to their nonlinear versions are also shown as a percentage. It is observed that the linearized LFS solver offers increasingly higher speed-ups with respect to the FS solver as the order of the numerical scheme is increased, for a fixed CFL number. While the 3rd order HLLSL-ADER and ARL-ADER schemes only save around a

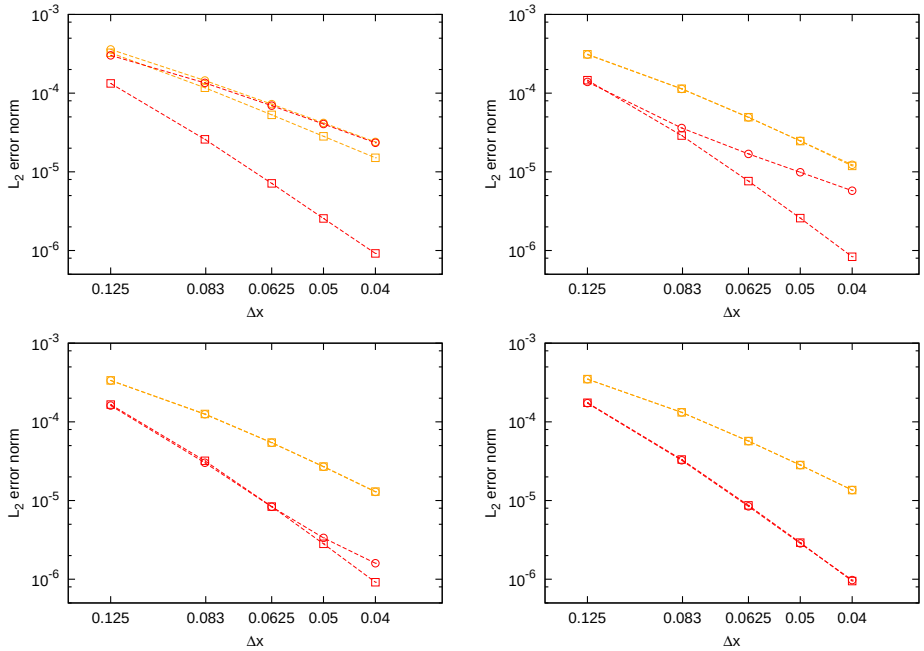

Figure 24: Section 6.5. L_1 error norm for the water depth h using the 3rd order HLLS-ADER scheme (−□−), the 3rd order HLLSL-ADER scheme (− ○ −) , the 5th order HLLS-ADER sheme (−□−) and the 5th order HLLSL-ADER sheme (− ○ −). Results computed setting CFL= 0.6 (upper left), CFL= 0.3 (upper right), CFL= 0.15 (lower left) and CFL= 0.08 (lower right).

10% of the computational time required for the HLLS-ADER and AR-ADER schemes, the 5th order schemes offer up to a 40% of computational time saving.

It is worth mentioning that the LFS solver avoids the computation of the Cauchy-Kowalevski procedure for the fluxes, which is a very tedious and expensive process regarding CPU time. The expression for the time derivatives of the fluxes, obtained by means of the Cauchy-Kowalevski procedure, become exponentially larger as the required order of accuracy is increased. That is why much larger CPU time saving is shown in Table 11 for the 5th order LFS-based schemes than for the 3rd order schemes. When using the LFS solver, CPU time saving is expected to increase as the order of accuracy of the scheme is increased. Therefore, when moving to very high order of accuracy, it may be more efficient to use a LFS-based scheme with a low CFL number than a FS-based scheme with higher CFL number. This issue

		h				q			
Scheme	N	L_1 error	Order	L_2 error	Order	L_1 error	Order	L_2 error	Order
1st order	40	3.71E-03		1.01E-03		7.36E-03		2.07E-03	
	60	2.84E-03	0.66	6.53E-04	1.07	5.81E-03	0.58	1.38E-03	1.00
	80	2.32E-03	0.70	4.68E-04	1.16	4.84E-03	0.64	1.01E-03	1.10
	100	1.95E-03	0.78	3.57E-04	1.22	4.11E-03	0.73	7.75E-04	1.17
	125	1.63E-03	0.80	2.70E-04	1.23	3.49E-03	0.76	5.90E-04	1.20

Table 2: Convergence rate test for h and q using L_1 and L_2 error norms for the 1st order Godunov scheme. CFL=0.3.

		h				q			
Scheme	N	L_1 error	Order	L_2 error	Order	L_1 error	Order	L_2 error	Order
3rd order	40	1.02E-03		3.00E-04		2.73E-03		7.64E-04	
	60	4.77E-04	1.87	1.09E-04	2.49	1.12E-03	2.20	2.56E-04	2.70
	80	2.30E-04	2.54	4.68E-05	2.95	5.22E-04	2.65	1.06E-04	3.06
	100	1.27E-04	2.65	2.31E-05	3.17	2.86E-04	2.70	5.15E-05	3.24
	125	6.72E-05	2.86	1.10E-05	3.30	1.48E-04	2.95	2.44E-05	3.35
5th order	40	5.57E-04		1.45E-04		1.13E-03		3.00E-04	
	60	1.28E-04	3.63	2.77E-05	4.08	2.36E-04	3.85	5.30E-05	4.27
	80	3.59E-05	4.41	7.19E-06	4.68	6.45E-05	4.51	1.30E-05	4.89
	100	1.30E-05	4.57	2.40E-06	4.92	2.30E-05	4.62	4.09E-06	5.17
	125	4.47E-06	4.78	7.65E-07	5.13	7.23E-06	5.19	1.25E-06	5.31

Table 3: Convergence rate test for h and q using L_1 and L_2 error norms for the 3rd and 5th order asymptotically energy balanced AR-ADER scheme. CFL=0.3.

is to be explored in the future.

7. Summary and concluding remarks

In this work, arbitrary order finite volume numerical schemes of the flux-ADER type based on an augmented solvers have been studied. These schemes are constructed using the flux-ADER methodology, that is, the numerical fluxes at the interfaces are directly computed by means of a Taylor power series expansion in time. The coefficients for the power expansion of the numerical flux are computed by solving the DRP.

A wide variety of solvers can be used for the resolution of the DRP, however, most of them do not consider the presence of the source term in the solution. In this work, the FS Derivative Riemann solver, used for the first time in [1], is recalled and used to construct a novel scheme. This solver was constructed as a natural arbitrary order extension of the ARoe solver

		h				q			
Scheme	N	L_1 error	Order	L_2 error	Order	L_1 error	Order	L_2 error	Order
3rd order	40	1.10E-03		3.12E-04		2.83E-03		7.76E-04	
	60	4.97E-04	1.96	1.14E-04	2.48	1.17E-03	2.18	2.64E-04	2.66
	80	2.42E-04	2.50	4.94E-05	2.92	5.46E-04	2.65	1.10E-04	3.04
	100	1.35E-04	2.63	2.46E-05	3.13	2.99E-04	2.70	5.38E-05	3.22
	125	7.40E-05	2.69	1.19E-05	3.25	1.60E-04	2.81	2.56E-05	3.32
5th order	40	5.44E-04		1.46E-04		1.15E-03		3.14E-04	
	60	1.35E-04	3.45	2.89E-05	4.00	2.54E-04	3.73	5.59E-05	4.25
	80	3.84E-05	4.35	7.62E-06	4.63	6.96E-05	4.50	1.38E-05	4.86
	100	1.42E-05	4.46	2.58E-06	4.86	2.57E-05	4.46	4.41E-06	5.11
	125	5.03E-06	4.66	8.34E-07	5.06	8.54E-06	4.94	1.35E-06	5.30

Table 4: Convergence rate test for h and q using L_1 and L_2 error norms for the 3rd and 5th order asymptotically energy balanced HLLS-ADER scheme. CFL=0.3.

		h				q			
Scheme	N	L_1 error	Order	L_2 error	Order	L_1 error	Order	L_2 error	Order
3rd order	40	1.21E-03		3.54E-04		3.22E-03		8.99E-04	
	60	5.75E-04	1.84	1.34E-04	2.40	1.31E-03	2.22	3.06E-04	2.66
	80	2.88E-04	2.40	5.80E-05	2.91	6.41E-04	2.48	1.29E-04	3.00
	100	1.59E-04	2.66	2.88E-05	3.14	3.50E-04	2.72	6.33E-05	3.19
	125	8.47E-05	2.83	1.38E-05	3.28	1.84E-04	2.88	3.02E-05	3.32
5th order	40	7.11E-04		1.78E-04		1.32E-03		3.37E-04	
	60	1.50E-04	3.84	3.33E-05	4.13	2.66E-04	3.96	6.40E-05	4.09
	80	4.38E-05	4.28	8.67E-06	4.68	7.89E-05	4.22	1.60E-05	4.81
	100	1.57E-05	4.59	2.91E-06	4.90	2.79E-05	4.65	5.17E-06	5.07
	125	5.75E-06	4.50	9.50E-07	5.01	9.56E-06	4.80	1.61E-06	5.23

Table 5: Convergence rate test for h and q using L_1 and L_2 error norms for the 3rd and 5th order asymptotically energy balanced ARL-ADER scheme. CFL=0.05.

		h				q			
Scheme	N	L_1 error	Order	L_2 error	Order	L_1 error	Order	L_2 error	Order
3rd order	40	1.21E-03		3.54E-04		3.22E-03		8.99E-04	
	60	5.75E-04	1.84	1.34E-04	2.40	1.31E-03	2.22	3.06E-04	2.66
	80	2.88E-04	2.40	5.80E-05	2.91	6.41E-04	2.48	1.29E-04	3.00
	100	1.59E-04	2.66	2.88E-05	3.14	3.50E-04	2.72	6.33E-05	3.19
	125	8.47E-05	2.83	1.38E-05	3.28	1.84E-04	2.88	3.02E-05	3.32
5th order	40	7.11E-04		1.78E-04		1.32E-03		3.37E-04	
	60	1.50E-04	3.84	3.33E-05	4.13	2.66E-04	3.96	6.40E-05	4.09
	80	4.38E-05	4.28	8.67E-06	4.68	7.89E-05	4.22	1.60E-05	4.81
	100	1.57E-05	4.59	2.91E-06	4.90	2.79E-05	4.65	5.17E-06	5.07
	125	5.75E-06	4.50	9.50E-07	5.01	9.56E-06	4.80	1.61E-06	5.23

Table 6: Convergence rate test for h and q using L_1 and L_2 error norms for the 3rd and 5th order asymptotically energy balanced HLLSL-ADER scheme. CFL=0.05.

		h				q			
Scheme	N	L_1 error	Order	L_2 error	Order	L_1 error	Order	L_2 error	Order
3rd order	40	1.02E-03		3.00E-04		2.74E-03		7.67E-04	
	60	4.78E-04	1.87	1.09E-04	2.49	1.12E-03	2.19	2.57E-04	2.69
	80	2.30E-04	2.54	4.69E-05	2.95	5.27E-04	2.64	1.07E-04	3.05
	100	1.27E-04	2.65	2.31E-05	3.16	2.89E-04	2.69	5.21E-05	3.22
	125	6.77E-05	2.83	1.11E-05	3.30	1.51E-04	2.91	2.48E-05	3.33
5th order	40	5.58E-04		1.45E-04		1.13E-03		3.01E-04	
	60	1.28E-04	3.63	2.78E-05	4.07	2.39E-04	3.84	5.36E-05	4.25
	80	3.64E-05	4.38	7.26E-06	4.66	6.77E-05	4.39	1.34E-05	4.83
	100	1.32E-05	4.55	2.46E-06	4.85	2.49E-05	4.49	4.38E-06	5.00
	125	4.80E-06	4.54	8.30E-07	4.87	8.98E-06	4.56	1.46E-06	4.94

Table 7: Convergence rate test for h and q using L_1 and L_2 error norms for the 3rd and 5th order energy balanced AR-ADER scheme. CFL=0.3.

		h				q			
Scheme	N	L_1 error	Order	L_2 error	Order	L_1 error	Order	L_2 error	Order
3rd order	40	1.10E-03		3.12E-04		2.84E-03		7.78E-04	
	60	4.97E-04	1.96	1.14E-04	2.48	1.18E-03	2.17	2.66E-04	2.65
	80	2.42E-04	2.50	4.93E-05	2.92	5.49E-04	2.65	1.11E-04	3.04
	100	1.35E-04	2.62	2.45E-05	3.13	3.02E-04	2.67	5.41E-05	3.21
	125	7.37E-05	2.71	1.18E-05	3.27	1.61E-04	2.81	2.58E-05	3.33
5th order	40	5.46E-04		1.46E-04		1.16E-03		3.15E-04	
	60	1.35E-04	3.45	2.89E-05	4.00	2.57E-04	3.71	5.64E-05	4.24
	80	3.81E-05	4.39	7.63E-06	4.63	7.19E-05	4.43	1.41E-05	4.82
	100	1.41E-05	4.47	2.58E-06	4.86	2.74E-05	4.33	4.60E-06	5.02
	125	4.98E-06	4.65	8.54E-07	4.96	9.54E-06	4.72	1.50E-06	5.01

Table 8: Convergence rate test for h and q using L_1 and L_2 error norms for the 3rd and 5th order energy balanced HLLS-ADER scheme. CFL=0.3.

		h				q			
Scheme	N	L_1 error	Order	L_2 error	Order	L_1 error	Order	L_2 error	Order
3rd order	40	1.21E-03		3.54E-04		3.23E-03		9.02E-04	
	60	5.75E-04	1.84	1.34E-04	2.39	1.31E-03	2.22	3.07E-04	2.66
	80	2.89E-04	2.39	5.81E-05	2.91	6.46E-04	2.47	1.30E-04	3.00
	100	1.60E-04	2.64	2.88E-05	3.14	3.54E-04	2.70	6.38E-05	3.18
	125	8.54E-05	2.82	1.39E-05	3.28	1.87E-04	2.85	3.05E-05	3.30
5th order	40	7.12E-04		1.78E-04		1.33E-03		3.38E-04	
	60	1.50E-04	3.84	3.34E-05	4.12	2.68E-04	3.95	6.45E-05	4.08
	80	4.45E-05	4.22	8.73E-06	4.67	8.10E-05	4.16	1.63E-05	4.77
	100	1.58E-05	4.64	2.94E-06	4.88	2.89E-05	4.61	5.33E-06	5.02
	125	5.87E-06	4.44	9.70E-07	4.97	1.04E-05	4.60	1.69E-06	5.13

Table 9: Convergence rate test for h and q using L_1 and L_2 error norms for the 3rd and 5th order energy balanced ARL-ADER scheme. CFL=0.05.

		h				q			
Scheme	N	L_1 error	Order	L_2 error	Order	L_1 error	Order	L_2 error	Order
3rd order	40	1.21E-03		3.54E-04		3.23E-03		9.02E-04	
	60	5.75E-04	1.84	1.34E-04	2.39	1.31E-03	2.22	3.07E-04	2.66
	80	2.89E-04	2.39	5.81E-05	2.91	6.46E-04	2.47	1.30E-04	3.00
	100	1.60E-04	2.64	2.88E-05	3.14	3.54E-04	2.70	6.38E-05	3.18
	125	8.54E-05	2.82	1.39E-05	3.28	1.87E-04	2.85	3.05E-05	3.30
5th order	40	7.12E-04		1.78E-04		1.33E-03		3.38E-04	
	60	1.50E-04	3.84	3.34E-05	4.12	2.68E-04	3.95	6.45E-05	4.08
	80	4.45E-05	4.22	8.73E-06	4.67	8.10E-05	4.16	1.63E-05	4.77
	100	1.58E-05	4.64	2.94E-06	4.88	2.89E-05	4.61	5.33E-06	5.02
	125	5.87E-06	4.44	9.70E-07	4.97	1.04E-05	4.60	1.69E-06	5.13

Table 10: Convergence rate test for h and q using L_1 and L_2 error norms for the 3rd and 5th order energy balanced HLLSL-ADER scheme. CFL=0.05.

		HLLSL-ADER		HLLS-ADER	ARL-ADER		AR-ADER
Cells	Order	Time (s)	Speed-up	Time (s)	Time (s)	Speed-up	Time (s)
160	3	2.00	11%	2.25	1.98	11%	2.22
	5	54.92	39%	90.62	54.55	40%	90.26
80	3	0.50	11%	0.57	0.50	15%	0.58
	5	13.54	40%	22.52	13.56	41%	22.85

Table 11: CPU times for test case in Section 6.5 at $t = 3$ s, setting CFL=0.3. Times are shown for the 3rd and 5th order energy balanced HLLSL-ADER, HLLS-ADER, ARL-ADER and AR-ADER schemes. Speed-ups of the HLLSL-ADER and ARL-ADER schemes with respect to their nonlinear version are shown as a percentage.

and allowed to construct an arbitrary order numerical scheme, namely the AR-ADER scheme, that ensured the energy balanced property when solving the SWE. The FS solver is designed to solve non-linear systems of PDEs with source term, in particular, with geometric source terms.

A simplification of the FS solver, called LFS solver and based on the linearization of the RPs corresponding to the derivatives, has been presented in this work. The main advantage of this novel approach is that only derivatives of the conserved quantities have to be reconstructed at the interfaces, unlike in the FS solver that also the reconstruction of derivatives of the fluxes was required. This simplification is done at the expense of stronger restrictions on the time step. Numerical results evidence that only when using CFL numbers below 0.1 the numerical scheme using the LFS solver achieves the prescribed accuracy. It is worth recalling that numerical schemes using the original FS solver converge at the expected rate for higher CFL numbers.

In the present work, a novel numerical scheme that uses the FS and LFS solvers in combination with the HLLS Riemann solver has been presented. The resulting method is called HLLS-ADER scheme. Numerical results show that both, the AR-ADER and HLLS-ADER schemes, have a similar performance. When applied to the SWE, the AR-ADER and HLLS-ADER schemes and their linearized versions can be energy balanced, providing the exact solution in steady cases with independence of the grid and ensuring convergence to the exact solution at the prescribed rate for transient problems. Otherwise, they can be asymptotically energy balanced, but convergence to the exact solution will still be guaranteed. To check this, the numerical schemes have been thoroughly assessed using a variety of steady and transient test cases.

It has been pointed out in the text that when constructing high order energy balanced schemes, energy considerations must not only have to be taken into account in the discretization of the source term at cell interfaces for the RPs but also when approaching the integral of the source term inside the cell. In this work we have studied two alternatives for the integration of the source term that allow to, at least, converge to the exact solution. It is worth saying that both alternatives require energy balance discretization of the source term [49] at cell interfaces when solving the RPs. The first option is to compute the integral of the source term using traditional quadrature rules, for instance, Gaussian quadrature. The second possibility is to extrapolate the energy balanced discretization technique in [49], as proposed by Noelle [45], to construct an arbitrary order approximation of the integral. For steady

cases, while the former approach only allows convergence to the exact solution when the grid is refined, the latter makes the numerical scheme to directly provide the exact solution with independence of the grid. When applied to transient cases, both approaches have proven to provide similar solutions. It has been noticed a slightly faster convergence rate for the asymptotically energy balanced schemes since the approximation of the integral of the source term inside the cell is optimal in which refers to accuracy. However, it is preferable to use an exact energy balanced scheme even when obtaining a slightly slower convergence rate, since it will always provide the exact solution under steady state.

In this work, numerical results for the resolution of the SWE have been included to evidence the previously mentioned features of the numerical schemes and their rates of convergence. When carrying out convergence rate tests, numerical errors have been computed by comparing with a high order numerical solution calculated in a very fine mesh. It must be borne in mind that the use of manufactured solutions may not be adequate since they are useful to prove the accuracy of the numerical scheme but they do not allow to check if the scheme converges to a physically based solution.

References

[1] A. Navas-Montilla, J. Murillo, Energy balanced numerical schemes with very high order. The Augmented Roe Flux ADER scheme. Application to the shallow water equations, J. Comput. Phys. 290 (2015) 188–218.

[2] A. Harten, B. Engquist, S. Osher, S.R. Chakravarthy, Uniformly high order accuracy essentially non-oscillatory schemes III, J. Comput. Phys. 71 (1987) 231–303.

[3] X.-D. Liu, S. Osher, T. Chan, Weighted essentially non-oscillatory schemes, J. Comput Phys. 115 (1994) 200–212.

[4] T. Schwartzkopff, M. Dumbser, C.-D. Munz, Fast high order ADER schemes for linear hyperbolic equations, J. Comput. Phys. 197 (2004) 532–539.

[5] E.F. Toro, R.C. Millington, and L.A.M. Nejad. Primitive upwind methods for hyperbolic partial differential equations. In C. H. Bruneau, editor, Sixteenth International Conference on Numerical Methods for Fluid

Dynamics. Lecture Notes in Physics, pages 421–426. Springer-Verlag, 1998.

[6] E.F. Toro, R.C. Millington, and L.A.M. Nejad. Towards very high order Godunov schemes. In E. F. Toro, editor, Godunov Methods. Theory and Applications, pages 907–940. Kluwer/Plenum Academic Publishers, 2001.

[7] E.F. Toro, V.A. Titarev, Solution of the generalised Riemann problem for advection-reaction equations, Proc. Roy. Soc. London A 458 (2002) 271–281.

[8] E.F. Toro, V.A. Titarev, ADER schemes for scalar hyperbolic conservation laws with source terms in three space dimensions, J. Comput. Phys. 202 (1) (2005) 196–215.

[9] E.F. Toro, V.A. Titarev, Derivative Riemann solvers for systems of conservation laws and ADER methods, J. Comput Phys. 212 (1) (2006) 150–165.

[10] M. Ben-Artzi, J. Falcovitz. A second order Godunov-type scheme for compressible fluid dynamics, J. Comput. Phys. 55 (1984) 1–32.

[11] C.E. Castro, E.F. Toro, Solvers for the high-order Riemann problem for hyperbolic balance laws, J. Comput. Phys. 227 (2008) 2481–2513.

[12] E.F. Toro, G. Montecinos, Implicit, semi-analytical solution of the generalized Riemann problem for stiff hyperbolic balance laws, J. Comput. Phys. 303 (2015) 146–172.

[13] M. Dumbser, C. Enaux, E.F. Toro, Finite volume schemes of very high order of accuracy for stiff hyperbolic balance laws, J. Comput. Phys. 227 , Issue (2008) 3971–4001.

[14] J. Murillo, P. García-Navarro, Weak solutions for partial differential equations with source terms: application to the shallow water equations, J. Comput. Phys. 229 (2010) 4327–4368.

[15] E.F. Toro, Riemann solvers and numerical methods for fluid dynamics: a practical introduction, third ed., Springer-Verlag, Berlin, Heidelberg, 2009.

[16] C.E. Castro, E.F. Toro and M. Käser, ADER scheme on unstructured meshes for shallow water: simulation of tsunami waves, Geophys. J. Int. 189 (2021) 1505–1520.

[17] G. Vignoli, V.A. Titarev, E.F. Toro, ADER schemes for the shallow water equations in channel with irregular bottom elevation, J. Comput. Phys. 227 (2008) 2463–2480.

[18] G. Montecinos, C.E. Castro, M. Dumbser and E.F. Toro, Comparison of solvers for the generalized Riemann problem for hyperbolic systems with source terms, J. Comput. Phys. 231 (2012) 6472 – 6494.

[19] D.L. George. Augmented Riemann solvers for the shallow water equations over variable topography with steady states and inundation, J. Comput. Phys. 227 (2008) 3089–3113.

[20] J. Murillo, J. Burguete, P. Brufau, and P. García-Navarro. The influence of source terms on stability, accuracy and conservation in two-dimensional shallow flow simulation using triangular finite volumes, Int. J. Numer. Meth. Fluids (2007) 54 543–590.

[21] J. Murillo, P. García-Navarro, Augmented Roe's approaches for Riemann problems including source terms: definition of stability region with application to the shallow water equations with rigid and deformable bed. In M. E. Vázquez-Cendón and A. Hidalgo and P. García-Navarro and L. Cea, eds., Numerical Methods for Hyperbolic Equations. Theory and Applications, pages 149–154. Taylor-Francis Group, 2013.

[22] P.L. Roe, Approximate Riemann solvers, parameter vectors, and difference schemes, J. Comput. Phys. 43 (1981) 357–372.

[23] A. Harten, P. Lax and B. van Leer, On upstream differencing and Godunov type methods for hyperbolic conservation laws, SIAM review. 25 (1983) 35–61.

[24] E.F. Toro, M. Spruce, W. Spears, Restoration of the contact surface in the HLL Riemann solver, Shock Waves. 4 (1994) 25–34.

[25] J. Murillo, P. García-Navarro, Augmented versions of the HLL and HLLC Riemann Solvers including source terms in one and two dimensions for shallow flow applications, J. Comput. Phys. 231 (2012) 6861–6906.

[26] A. Bermudez and M.E. Vázquez-Cendón, Upwind methods for hyperbolic conservation laws with source terms, Comput. Fluids. 23 (1994) 1049–1071.

[27] J.M. Greenberg, A.Y. Leroux, A well-balanced scheme for the numerical processing of source terms in hyperbolic equations, SIAM J. Numer. Anal. 33 (1996) 1–16.

[28] P. García-Navarro, M.E. Vázquez-Cendón. On numerical treatment of the source terms in the shallow water equations, Comput. and Fluids. 29 (2000) 951–979.

[29] J. Burguete and P. García-Navarro. Efficient construction of high-resolution TVD conservative schemes for equations with source terms: application to shallow water flows, Int. J. Numer. Meth. Fluids 37 (2001) 209–248.

[30] J. Burguete and P. García-Navarro. Implicit schemes with large time step for non-linear equations: application to river flow hydraulics, Int. J. Numer. Meth. Fluids 46 (2004) 607–636.

[31] A. Chinnayya, A.-Y. LeRoux, N. Seguin, A well-balanced numerical scheme for the approximation of the shallow water equations with topography: the resonance phenomenon, Int. J. Finite Vol. 1 (2004) 1–33.

[32] R. Bernetti, V.A. Titarev, E.F. Toro, Exact solution of the Riemann problem for the shallow water equations with discontinuous bottom geometry, J. Comput. Phys. 227 (2008) 3212–3243.

[33] G. Rosatti, L. Begnudelli, The Riemann Problem for the one-dimensional, free-surface Shallow Water Equations with a bed step: theoretical analysis and numerical simulations, J. Comput. Phys. 229 (2010) 760-787.

[34] P.G. LeFloch, M.D. Thanh, The Riemann problem for shallow water equations with discontinuous topography, Commun. Math. Sci. 5 (2007) 865–885.

[35] P.G. LeFloch, M.D. Thanh, A Godunov-type method for the shallow water equations with discontinuous topography in the resonant regime, J. Comput. Phys. 230 (2011) 7631–7660.

[36] X. Yulong and S. Chi-Wang , High order finite difference WENO schemes with the exact conservation property for the shallow water equations, J. Comput. Phys. 208 (2005) 206–227.

[37] F. Alcrudo, F. Benkhaldoun, Exact solutions to the Riemann problem of the shallow water equations with a bottom step, Comput. Fluids 30 (2001) 643–671.

[38] B.F. Sanders, D.A. Jaffe and A.K. Chu. Discretization of integral equations describing flow in nonprismatic channels with uneven beds, J. Hydraul. Eng–ASCE 129(3) (2003) 235–244.

[39] G. Kesserwani, R. Ghostine, J. Vazquez, A. Ghenaim and R. Mosé. Application of a second-order Runge-Kutta discontinuous Galerkin scheme for the shallow water equations with source terms, Int. J. Numer. Meth. Fluids 56 (2008) 805–821.

[40] M. Catella, E. Paris and L. Solari. Conservative scheme for numerical modeling of flow in natural geometry, J. Hydraul. Eng–ASCE 134(6) (2008) 736–748.

[41] S.H. Lee and N.G. Wright. Simple and efficient solution of the shallow water equations with source terms, Int. J. Numer. Meth. Fluids 63 (2010) 313–340.

[42] V. Caleffi, A. Valiani, G. Li, A comparison between bottom-discontinuity numerical treatments in the DG framework, Appl. Math. Model. (2015).

[43] M.E. Vázquez-Cendón. Improved treatment of source terms in upwind schemes for the shallow water equations in channels with irregular geometry, J. Comput. Phys. 148 (1999) 497–498.

[44] P. Brufau, M.E. Vázquez-Cendón and P. García-Navarro. A numerical model for the flooding and drying of irregular domains, Int. J. Numer. Meth. Fluids 39 (2002) 247–275.

[45] Noelle, S., Xing, Y. and Shu, C., High-order well-balanced finite volume WENO schemes for shallow water equation with moving water, J. Comput. Phys. 226 (2007) 29–58.

[46] U.S. Fjordholm, S. Mishra, E. Tadmor,Well-balanced and energy stable schemes for the shallow water equations with discontinuous topography, J. Comput. Phys. 230 (2011) 5587–5609.

[47] M.J. Castro Díaz , J.A. López-García, Carlos Parés, High order exactly well-balanced numerical methods for shallow water systems, J. Comput. Phys. 246 (2013) 242–264.

[48] Y. Xing,Exactly well-balanced discontinuous Galerkin methods for the shallow water equations with moving water equilibrium, J. Comput. Phys. 257 (2014) 536–553.

[49] J. Murillo, P. García-Navarro, Energy balance numerical schemes for shallow water equations with discontinuous topography, J. Comput. Phys. 236 (2012) 119–142.

[50] J. Murillo, P. García-Navarro, Accurate numerical modeling of 1D flow in channels with arbitrary shape. Application of the energy balanced property, J. Comput. Phys. 260 (2014) 222–248.

[51] P. Le Floch, P. A. Raviart. An Asymptotic Expansion for the Solution of the Generalized Riemann Problem. Part 1: General Theory. Ann. Inst. Henri Poincare. Analyse non Lineare, 5 (1988) 179–207.

[52] V. A. Titarev. Derivative Riemann Problem and ADER Schemes. PhD thesis, Department of Mathematics, University of Trento, Italy, 2005.

[53] S.K. Godunov, Finite difference methods for the computation of discontinuous solutions of the equations of fluid dynamics, Mat. Sb. 47 (1959) 271–306.

[54] J.B. Cheng, E. F. Toro, S. Jiang, W. Tang, A sub-cell WENO reconstruction method for spatial derivatives in the ADER scheme, J. Comput. Phys. 251 (2013) 53–80.

[55] R. Burden, J. Faires. Numerical analysis. Nelson Education (2015).